Degree Thesis for Doctor of Philosophy

Automatic Wi-Fi Fingerprint System based on Unsupervised Learning

Supervisor : Prof. Dong-Hoan Seo

August 2018

Department of Electrical and Electronics Engineering

The Graduate School of Korea Maritime and Ocean University

Ju-Hyeon Seong

Thesis submitted by Ju-Hyeon Seong in Fulfillment of Requirement for the Degree of Doctor of Philosophy

Committee Chairman : D. Eng. Yoon-Sik Kim ㊞

Committee Member : D. Eng. Hyung-Rae Cho ㊞

Committee Member : D. Eng. Yang-Ick Joo ㊞

Committee Member : D. Sci. Byung-Tae Jang ㊞

Committee Member : D. Eng. Dong-Hoan Seo ㊞

August 2018

Department of Electrical and Electronics Engineering

The Graduate School of Korea Maritime and Ocean University

Ju-Hyeon Seong

Contents

Lists of Figures and Tables

< List of Figures >

< List of Tables >

비지도학습 기반 자동 Wi-Fi Fingerprint 시스템

by Ju Hyeon Seong

Department of Electrical & Electronics Engineering

The Graduate School of Korea Maritime and Ocean University

Busan, Republic of Korea

Abstract

최근 스마트폰과 Wi-Fi가 실생활에 보편화되면서 위치기반 서비스에 대한 개발 분야가 실내 환경으로 점차 확대되고 있다. GPS로 대표되는 실외 위치 인식과 달리 위치기반 서비스를 제공하기 위한 실내 위치 인식 기술은 Wi-Fi, UWB, 블루투스 등과 같은 다양한 근거리 무선 통신 기반의 알고리즘들이 연구되고 있다.

대표적인 실내 위치인식 알고리즘 중 하나인 Fingerprint는 사용자가 수신한 AP 신호의 상대적인 크기를 나타내는 RSSI를 사용하여 위치를 추정한다. 따라서 Fingerprint기반의 알고리즘은 장애물이 많이 존재하는 비가시 거리에서 TOA 방식에 비해 전파의 반사 및 굴절과 같이 왜곡된 무선 환경에 강인하다는 장점이 있다. Fingerprint는 실내의 모든 AP의 RSSI들을 측정하여 Radio map을 제작하는 과정인 학습 단계와 생성된 Radio map의 RSSI들을 실시간으로 측정된 RSSI와 비교하여 사용자의 위치를 추정하는 위치인식 단계로 나누어진다. 학습 단계에서는 위치를 구분하기 위하여 사용자가 2~3m의 일정한 간격으로 설정된 참조 위치들마다 측정되는 모든 AP들의 RSSI를 수집하고 Radio map으로 제작한다. 위치인식 단계에서는 학습 단계에서 제작된 Radio map과 사용자의 이동에 의해 측정되는 RSSI의 비교를 통해 가장 유사한 RSSI 패턴을 가지는 참조 위치

가 실시간 실내 위치로 추정된다.

서포트 벡터 머신(SVM), 주성분 분석(PCA) 등과 같이 지도 및 준지도 학습 기반의 Fingerprint 알고리즘은 Radio map을 제작하기 위해 모든 실내 공간에서 RSSI의 측정이 필수적이다. 이러한 알고리즘들은 건물이 대형화되고 구조가 복잡해질수록 측정 공간이 늘어나면서 작업과 시간 소모가 또한 급격히 증가한다. 채널모델링을 통한 Radio map 생성 알고리즘은 직접적인 측정 과정이 불필요한 반면에 건물의 재질, 3차원적인 구조에 따른 반사 계수 및 모든 장애물에 대한 수치적인 모델링이 필수적이기 때문에 상당히 많은 작업량이 요구된다.

따라서 본 논문에서는 이러한 문제점들을 해결하고자 학습 단계에서 Wi-Fi 신호의 수집시간을 최소화하면서 실내 환경이 고려된 Unsupervised Dual Radio Mapping (UDRM) 알고리즘과 위치인식 단계에서 Radio map의 최적화가 동시에 가능한 Minimum description length principle (MDLP)기반의 Radio map Feedback (RMF) 알고리즘이 결합된 비지도학습기반의 자동 Wi-Fi Fingerprint를 제안한다. 학습 단계에서 제안하는 UDRM 알고리즘은 뉴럴 네트워크 기반의 비지도 학습 알고리즘인 Autoencoder와 Generative Adversarial Network (GAN)를 공간구조에 따라 선택적으로 적용하여 하나의 참조 층에서 측정된 Radio map을 기반으로 건물전체의 Radio map을 생성한다. 제안하는 비지도 학습 기반 UDRM 알고리즘은 지도 및 준지도 학습에서 필수적인 Labeled data가 필요하지 않으며 RSSI 데이터 세트의 의존성이 상대적으로 낮다. 또한 2차원 실내 지도를 통해 실내 환경을 동시에 학습하기 때문에 기존의 예측 모델에 비해 Radio map의 예측 정확도가 높다. 제안한 알고리즘에 의해 제작된 Radio map은 위치인식 단계에서 사용자의 실시간 위치인식에 적용된다. 동시에 제안하는 MDLP 기반의 자동 Wi-Fi 업데이트 알고리즘은 새롭게 측정되는 AP들의 RSSI의 분포특성을 분석하고 그 결과를 Radio map에 피드백한다. 제안한 알고리즘에 적용된 MDLP는 무분별한 RSSI의 업데이팅을 방지하고 추가되는 AP를 Radio map에 업데이트함으로서 위치인식의 성능을 향상시키고 Radio map의 크기의 최적화가 가능하다.

제안한 알고리즘은 실제 측정기반의 Radio map과 서로 비교를 통해 제안한 Fingerprint 시스템의 높은 안정성과 정확도를 확인하였다. 또한 구조가 다른 실내공간의 Radio map 생성 결과를 통해 실내 환경 변화에 강인함과 학습 시간 측정을 통한 시간 비용이 감소함을 확인하였다. 마지막으로 Euclidean distance 기반 실험을 통하여 실제 측정한 RSSI기반의 Fingerprint 시스템과 제안한 시스템의 위치인식 정확도가 거의 일치함을 확인하였다.

Automatic Wi-Fi Fingerprint System based on Unsupervised Learning

by Ju Hyeon, Seong

Department of Electrical & Electronics Engineering
Graduate School of Korea Maritime and Ocean University
Busan, Republic of Korea

Abstract

Recently, smartphones and Wi-Fi appliances have been generalized in daily life, and location-based service (LBS) has gradually been extended to indoor environments. Unlike outdoor positioning, which is typically handled by the global positioning system (GPS), indoor positioning technologies for providing LBSs have been studied with algorithms using various short-range wireless communications such as Wi-Fi, Ultra-wideband, Bluetooth, etc.

Fingerprint-based positioning technology, a representative indoor LBS, estimates user locations using the received signal strength indicator (RSSI), indicating the relative transmission power of the access point (AP). Therefore, a fingerprint-based algorithm has the advantage of being robust to distorted wireless environments, such as radio wave reflections and refractions, compared to the time-of-arrival (TOA) method for non-line-of-sight (NLOS),

where many obstacles exist. Fingerprint is divided into a training phase in which a radio map is generated by measuring the RSSIs of all indoor APs and positioning phase in which the positions of users are estimated by comparing the RSSIs of the generated radio map in real-time. In the training phase, the user collects the RSSIs of all APs measured at reference points set at regular intervals of 2 to 3 m, creating a radio map. In the positioning phase, the reference point, which is most similar to the RSSI, compares the generated radio map from the training phase to the RSSI measured from user movements. This estimates the real-time indoor position.

Fingerprint algorithms based on supervised and semi-supervised learning such as support vector machines and principal component analysis are essential for measuring the RSSIs in all indoor areas to produce a radio map. As the building size and the complexity of structures increases, the amount of work and time required also increase. The radio map generation algorithm that uses channel modeling does not require direct measurement, but it requires considerable effort because of building material, three-dimensional reflection coefficient, and numerical modeling of all obstacles. To overcome these problems, this thesis proposes an automatic Wi-Fi fingerprint system that combines an unsupervised dual radio mapping (UDRM) algorithm that reduces the time taken to acquire Wi-Fi signals and leverages an indoor environment with a minimum description length principle (MDLP)-based radio map feedback (RMF) algorithm to simultaneously optimize and update the radio map. The proposed UDRM algorithm in the training phase generates a radio map of the entire building based on the measured radio map of one reference floor by selectively applying the autoencoder and the generative

adversarial network (GAN) according to the spatial structures. The proposed learning-based UDRM algorithm does not require labeled data, which is essential for supervised and semi-supervised learning algorithms. It has a relatively low dependency on RSSI datasets. Additionally, it has a high accuracy of radio map prediction than existing models because it learns the indoor environment simultaneously via a indoor two-dimensional map (2-D map). The produced radio map is used to estimate the real-time positioning of users in the positioning phase. Simultaneously, the proposed MDLP-based RMF algorithm analyzes the distribution characteristics of the RSSIs of newly measured APs and feeds the analyzed results back to the radio map. The MDLP, which is applied to the proposed algorithm, improves the performance of the positioning and optimizes the size of the radio map by preventing the indefinite update of the RSSI and by updating the newly added APs to the radio map.

The proposed algorithm is compared with a real measurement-based radio map, confirming the high stability and accuracy of the proposed fingerprint system. Additionally, by generating a radio map of indoor areas with different structures, the proposed system is shown to be robust against the change in indoor environment, thus reducing the time cost. Finally, via a euclidean distance-based experiment, it is confirmed that the accuracy of the proposed fingerprint system is almost the same as that of the RSSI-based fingerprint system.

Chapter 1 Introduction

1.1 Background and Necessity for Research

Global positioning system (GPS)-based location based services (LBS) have applications in various fields such as the automotive industry, logistics, and security, etc. However, it is difficult to provide such services in indoor spaces because of the low signal transmittance of GPS. Recently, as the structures of buildings have become larger and more complex, the necessity of LBS in indoor environments has increased, and indoor positioning technologies, which can replace GPS, are being studied continuously [1, 2].

The representative indoor positioning methods are broadly classified into the time of arrival (TOA) [3-5], in which the distance between a transmitter and a receiver is estimated by measuring a signal arrival-time, and a fingerprint [6-9] in which a position is estimated by measuring an intensity of the relative signal of access point (AP) according to the indoor location.

Table 1.1 shows a comparison of the communication methods employed, advantages, and disadvantages of the fingerprint and TOA. The TOA, which includes the time difference of arrival (TDOA), a positioning technique of GPS, requires the signals to be received at three or more different points. And communication techniques or protocols that are capable of measuring the arrival time of the signal are also essential. Additionally, it requires the spatial positional coordinates of the transmitter because it estimates the positions of users using the relative distances between the transmitters and receivers.

Table 1.1 The comparison of fingerprint and TOA technology

Classification	Fingerprint	TOA
Communication technology	▪ Wi-Fi ▪ Zigbee ▪ Bluetooth low energy (BLE)	▪ Ultrawide-band (UWB) ▪ Chirp spread spectrum (CSS)
Advantages	▪ Robust to Non-line of sight (NLOS) ▪ High penetration rate	▪ High positioning resolution(*cm* unit) ▪ Low computational complexity
Disadvantages	▪ Long construction time of system ▪ Low positioning resolution(*m* unit)	▪ Large construction cost of system ▪ Vulnerability to disturbance (Refraction, Reflection, etc.)

The representative communication technologies of TOA are chirp spread spectrum (CSS) [10], ultrawide-band (UWB) [11,12], etc., and they have relatively higher positioning accuracies compared to the fingerprint. However, the cost of constructing such systems is many high because these communication systems are not universal radio systems.

Moreover, in the non-line-of-sight (NLOS) cases, where reflection and refraction of radio may occur, the position errors increase sharply because it will be difficult to measure the arrival time of the radio accurately.

The fingerprint has two phases. In the training phase, the intensities of the

radio signals measured at certain intervals in the indoor areas have generated a database called a “radio map”. In the positioning phase, the indoor positions of users is estimated based on the radio map generated in the training phase.

This method is suitable for most indoor communications such as Wi-Fi, BLE, and Zigbee [13-15], which can measure the received signal strength indicator (RSSI) that indicates the relative intensities of the radio signals measured according to the distance between a transmitter and a receiver. This method has the advantage that positioning is possible using the universal device alone, and does not require additional transmitters and receivers.

Wi-Fi, which is the most widely used short-range wireless communication technology, is a communication method that has been attracting attention in the field of positioning because of its longer transmission distance and stronger transmission power compared to other communications. Wi-Fi-based indoor positioning is applicable to both the fingerprint and trilateration which is the positioning technique of TOA [16].

If an indoor area has been analyzed perfectly (components of a medium, transmittance, multi-path fading, etc.), the trilateration, which identifies the position by converting the RSSI into a distance value that depends on the channel modeling of the radio, can predict the position accurately than the fingerprint.

On the other hand, the fingerprint does not need an analysis of the indoor radio environment in the training phase because it uses a radio map, which stores the RSSI as it is. However, the fingerprint requires more time for system preparation than the TOA because it is necessary to measure the Wi-Fi signal at each of positions called the “reference points” after dividing

the indoor space at regular intervals, in order to produce the radio map [17,18].

Therefore, as the size of the building and the density of Wi-Fi increases, the size and generation time of the radio map for positioning also increases rapidly. It is becoming increasingly necessary to find solutions to these problems, because they not only increase the time cost rapidly but also slow down the real-time positioning speed (in the case of fingerprint).

1.2 Objectives and Contents for Research

In order to reduce the time cost and workload, this thesis proposes an automatic Wi-Fi fingerprint system based on unsupervised learning that combines an unsupervised dual radio mapping (UDRM) algorithm, which reduces the acquisition time of the Wi-Fi signals and considers an indoor environment, and a minimum description length principle (MDLP)-based radio map feedback (RMF) algorithm to optimize and update the radio map simultaneously.

However, Wi-Fi needs to consider a spatial environment due to the large attenuation of RSSI depending on indoor area and structure. To solve this problem, the proposed UDRM algorithm, which is divided into a modified autoencoder and modified generative adversarial network (GAN), is separately applied to these algorithms, depending on whether the indoor structures of building is the same or different for floors. Using the measured radio map of one floor called a “reference floor“ in the building, the modified autoencoder predicts and generates the radio maps of other floors that have the same

structure as the reference floor. The signals set of Wi-Fi APs measured at each reference point, which is a fixed interval set to acquire the Wi-Fi signals in the building, is learned using the modified autoencoder as input data. The input data which is consist of service set identifiers (SSIDs) and the RSSIs can be directly applied to the other floors of the same structures because they learn the changed RSSI according to the reference points around the APs, using the autoencoder.

A modified GAN is applied to generate the radio maps for the other floors that have different indoor structures. The proposed modified GAN algorithm is designed to take in not only the Gaussian noise, which is the basic input signal but also a two-dimensional map (2-D map) and the coordinates of APs, as input data, to learn the indoor structure of the radio map. The designed input data are learned using a generator based on a neural network. When the learned data are input to a discriminator, along with the real measured radio map on the reference floor, the convolutional neural network (CNN) inside the discriminator compares and analyzes the space, placement of the APs, and entire RSSI distribution from the kernels which are filters of various sizes that can extract the characteristics of input data. The analyzed results of the discriminator are fed back to the generator. This process is repeated and the generator is gradually upgraded to an excellent learned generator that can similarly produce the real measured radio map. The modified GAN-based radio map at the new floors is generated through the learned generator by combining the 2-D map and the APs coordinates and various analyzed kernels data based on the real measured radio map at the reference floor. An entire radio map based on the proposed UDRM at the building is generated

by combining each radio map generated by selectively adapting the modified autoencoder and GAN.

Based on the entire radio map generated by the proposed UDRM algorithm, an MDLP-based RMF algorithm is proposed, to cope with not only the positioning but also the creation and removal of new APs in the positioning phase. The proposed MDLP-based RMF algorithm reduces the acquisition time of Wi-Fi RSSI through post-processing, by subordinating the measuring process of the RSSI in the training phase to the positioning phase. The MDLP, which is a discretization algorithm that discriminates and segments the continuity between the APs or RSSIs, preferentially removes the APs or RSSIs that have similar RSSI distributions because the coordinates of APs are spatially close and the RSSIs are not clearly distinguished according to the reference points. Using this algorithm, it is possible to manage the radio map continuously while preventing and reducing the indiscriminate updating of the radio map.

Chapter 2 Wi-Fi Positioning and Unsupervised Learning

2.1 Wi-Fi Positioning

2.1.1 Wi-Fi Signal and Fingerprint

Wi-Fi, which uses information such as the SSID, RSSI, channel, and security type, is used frequently along with various indoor wireless communication technologies such as Bluetooth and Zigbee, because it uses the industrial, scientific, and medical (ISM) frequency-bands of 2.4 GHz and 5 GHz. The RSSIs of these communications are further distorted by reflection and diffraction from obstacles such as walls, doors, and rooms, as well as by the general signal attenuation over distance. Generally, the RSSI, which is attenuated in air can be estimated using the log-distance path loss model of equation (2.1) [19].

$$P(r) = P(r_0) - 10n\log(\frac{r}{r_0}) + X_g \tag{2.1}$$

Where, r is the distance between the AP and the moving object, r_0 is the reference distance, X_g is a normal random variable with zero means, reflecting the attenuation, and n is the coefficient of the path loss. The path loss coefficient n represents an environmental variable determined according to the surrounding communication and indoor environment. This is applied to adjust

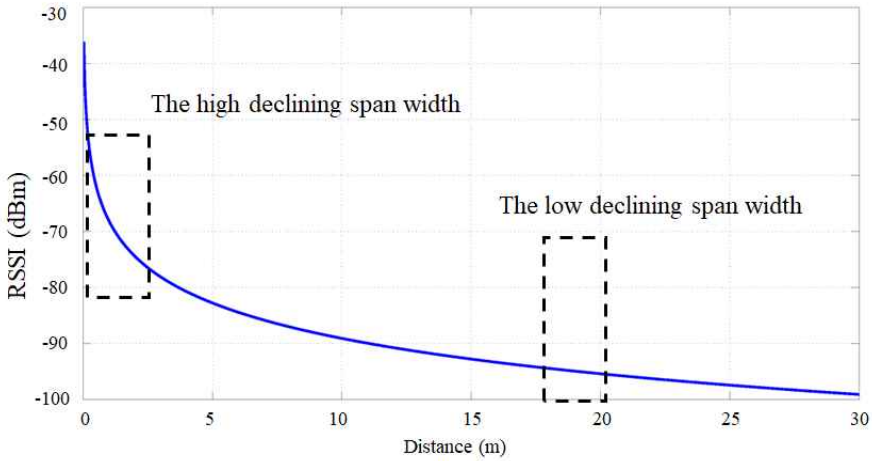

Fig. 2.1 The conventional attenuation of RSSI over distance

the path loss according to the surrounding medium, i.e., the indoor or outdoor conditions where the radio is measured.

Fig. 2.1 shows the conventional attenuation of RSSI over distance between a transmitter and a receiver. The x-axis represents the relative distance between the transmitter and receiver, and the y-axis represents the RSSIs of the transmitter measured by the receiver. As the relative distance increases, the less the change in declining span width is as shown in the Fig. 2.1. Therefore, The log-distance path loss model, which indicates the variation of the RSSI according to the distance, finds it difficult to distinguish the distance because the RSSI gradually becomes weaker as the relative distance between the transmitter and receiver increases.

As shown in Table 2.1, there are 14 frequency channels available for indoor wireless devices. However, as the penetration rate of smart devices increases, the indoor density of Wi-Fi per unit area also increases. Therefore, as the 14

Table 2.1 The frequency allocation of 2.4 Ghz Wi-Fi

Wi-Fi channels	Intermediate frequency (Ghz)	Channel frequency range (Ghz)
1	2.412	2.401 ~ 2.423
2	2.417	2.406 ~ 2.428
3	2.422	2.411 ~ 2.433
4	2.427	2.416 ~ 2.438
5	2.432	2.421 ~ 2.443
6	2.437	2.426 ~ 2.448
7	2.442	2.431 ~ 2.453
8	2.447	2.436 ~ 2.458
9	2.452	2.441 ~ 2.463
10	2.457	2.446 ~ 2.468
11	2.462	2.451 ~ 2.473
12	2.467	2.456 ~ 2.478
13	2.472	2.461 ~ 2.483
14	2.484	2.473 ~ 2.495

channels become saturated, many devices will use the same channel. If the AP density is high, despite the optimized frequency distribution, interference between the same or adjacent channels will occur.

Fig. 2.2 shows the Wi-Fi protocol applied to minimize the interference and collision of wireless communication, with a CSMA/CA protocol. The CSMA/CA is a typical medium-access method of the IEEE 802.11 wireless communication network (Wi-Fi), and is designed to avoid signal collisions between wireless devices. DIFS and SIFS, which indicate the time intervals

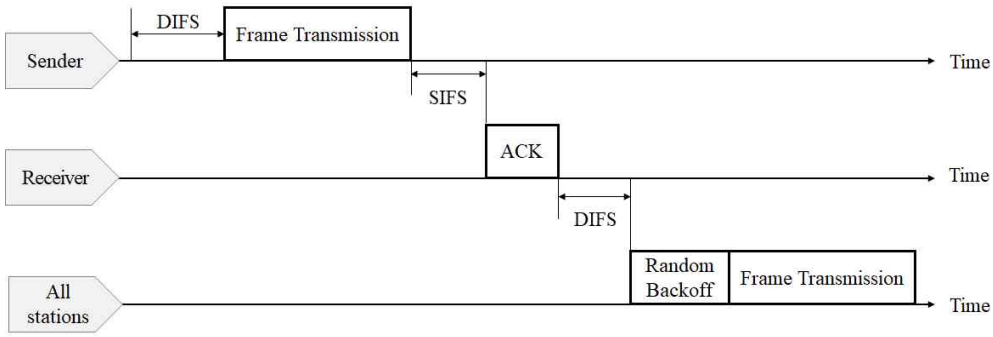

Fig. 2.2 The structure of CSMA/CA

between frames, are used to the receiver to detect the signal of receivers and avoid communication collisions with other senders, immediately before communicating with a connected sender. If it is determined that communication with another sender does not occur during a certain time interval, data communication occurs between the sender and receiver. When data are transmitted by multiple senders to the receiver, the senders wait and retransmit after a random back-off time, to prevent collisions from simultaneous transmissions. Since this protocol prevents data collisions in the same channel, information such as the SSID and RSSI of Wi-Fi devices using the same frequency band can be independently divided and measured according to APs. However, because many wireless devices share a single frequency, the waiting time for data transmission is long for CSMA/CA, which causes a speed reduction phenomenon [20, 21].

Even if the RSSIs are clearly different for the APs in which the channels overlap, the RSSI measured by the receiver has an irregular value with constant amplitude with respect to real-time. The reason for this is mainly the variation of the RSSI, which is distorted according to the structure or

material of the indoor area, and an inherent error caused by the hardware of the sender and receiver or the characteristics of the Wi-Fi frequency band, which has a high diffraction property. This is an important reason that reduces the user's positioning accuracy in the fingerprint. As the physical distance which is mean the interval of the reference point that can identify the position increases, the positioning resolution that can express the real position of the user, is reduced. Because the fluctuation of RSSI differs depending on the indoor environment, it is necessary to derive the physical distance over which the RSSI can be distinguished by measuring the basic signal and apply the optimized fingerprint unique to the environment and structure. The disadvantage of this Wi-Fi RSSI is that the positioning resolution that can represent the position is reduced to *m* units, compared to the TOA, which can recognize the position in *cm* units. However, compared to the TOA, the fingerprint has many advantages in indoor environments, such as large Wi-Fi scalability, low construction cost, and no requirement for separate receiver [22].

Fig. 2.3 shows the structure of the conventional fingerprint technique. The fingerprint technique is divided into the training phase that generates the radio map and the positioning phase that performs the positioning in real-time. The training phase generates the radio map using the measured RSSI for each reference point, set at regular intervals of 2 to 3 *m*, in order to position the user's location. The Wi-Fi signals measured at the reference point are used to generate the radio map through preprocessing such as averaging or partition of RSSIs that are attenuated by the relative distance between the transmitter and receiver, and surrounding structures. The RSSI,

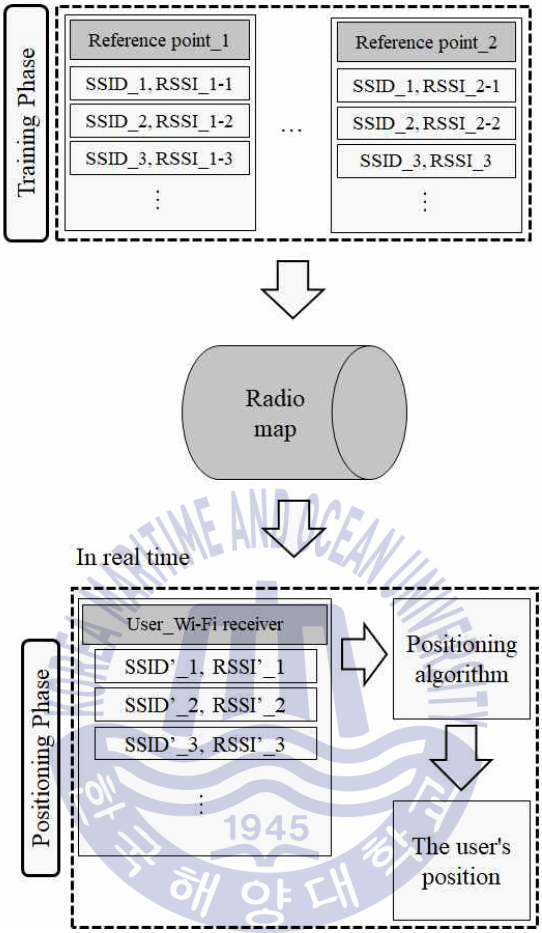

Fig. 2.3 The structure of conventional fingerprint

which is influenced by the relative distance and presence of obstacles, is an important value for positioning the user's location. The more accurate the classification of the RSSI of the AP measured according to each reference point is, the higher the accuracy of the positioning will be.

Fig. 2.4 shows the structure of the conventional radio map. The x-axis represents the RSSI of an arbitrary SSID, according to the changes in the reference point, and the y-axis represents all the measured APs at any one

$$D_{RM} = \begin{bmatrix} R_{SSID1(RP1)} & R_{SSID1(RP2)} & R_{SSID1(RP3)} & \cdots & R_{SSID1(RPn)} \\ R_{SSID2(RP1)} & R_{SSID2(RP2)} & R_{SSID2(RP3)} & \cdots & R_{SSID2(RPn)} \\ R_{SSID3(RP1)} & R_{SSID3(RP2)} & R_{SSID3(RP3)} & \cdots & R_{SSID3(RPn)} \\ \vdots & \vdots & \vdots & \vdots & \vdots \\ R_{SSID4(RP1)} & R_{SSID4(RP2)} & R_{SSID4(RP3)} & \cdots & R_{SSID4(RPn)} \end{bmatrix}$$

Fig. 2.4 The structure of conventional radio map

reference point. Since the x-axis is the reference point set of the entire area for positioning, the size of the x-axis will be constant according to the size of the area, irrespective of whether or not the RSSI of a specific AP is received at all reference points. On the other hand, since the y-axis indicates the number of APs, the larger the number of measured APs in space is, the larger the size of the radio map will be. Therefore, the x-axis, which is determined according to the indoor environment such as size and structures, can be determined according to the number of reference points; however, it will be difficult to reduce the reference points. Since the y-axis can control the number of APs, it is necessary to design a system that minimizes the APs and exhibits a high accuracy of positioning.

Fig. 2.5 shows the placement of the reference points, which are indicated by circles set at intervals of $2 \sim 3\,m$, and APs on the indoor map. According to the reference points, the SSID and RSSI of the Wi-Fi are measured several times, and the result of summarizing the measured Wi-Fi signals is called the radio map. Generally, the RSSI of any one AP is not measured at all reference points because one Wi-Fi cannot cover the entire indoor area. However, since the radio map must contain information about all reference

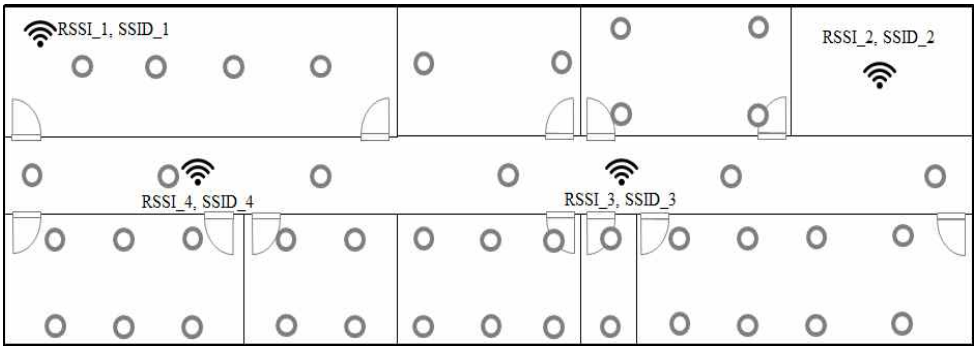

Fig. 2.5 The placement of reference points

points, the matrix of the radio map is given by [the number of reference points x the number of APs]. Therefore, even if only one AP is installed in the indoor area, the matrix of the radio map will be increased by [the number of reference points x 1].

In the positioning phase, the real-time position is estimated by comparing the radio map produced in the training phase with the measured Wi-Fi RSSI from the user's receiver. The RSSIs measured in real-time while the user is moving have reference points with similar RSSIs in the previously created radio map. The RSSIs measured by the user in real-time estimate the reference point with the highest similarity, from among the reference points with similar distributions in the previously created radio map, as the user 's location. In this method, since the reference point can be expressed by the user's position only, the positioning performance is determined according to the intervals of the reference point. Therefore, since the fingerprint method estimates the position based on the similarity of RSSIs, probabilistic or deterministic algorithms are applied [23]. Among them, the euclidean distance algorithm based on a k-nearest neighbor (K-NN), which is a non-parametric

method used for classification and regression, is often used for real-time multi-positioning because it is relatively uncomplicated for computation. The euclidean distance algorithm is as follows.

$$P = \min\left(\sqrt{\sum_{j=1}^{n}(AP_j - AP_{rj})^2}\right) \tag{2.2}$$

Here, P is the final position of the user, r is the measured real-time, and AP_j is the RSSI at the reference point j of the radio map. The reference point with the highest similarity is identified as the current position of the user by comparing AP_{rj}, which represents the RSSIs measured in real-time, and AP_j, which represents the RSSIs at all stored reference points in the radio map [24, 25]. Therefore, fingerprint, which is highly dependent on the radio map, requires much time cost and workload to implement the system in the training phase. The kinds of applied techniques are also highly varied when compared to the positioning phase.

2.1.2 Fingerprint Techniques

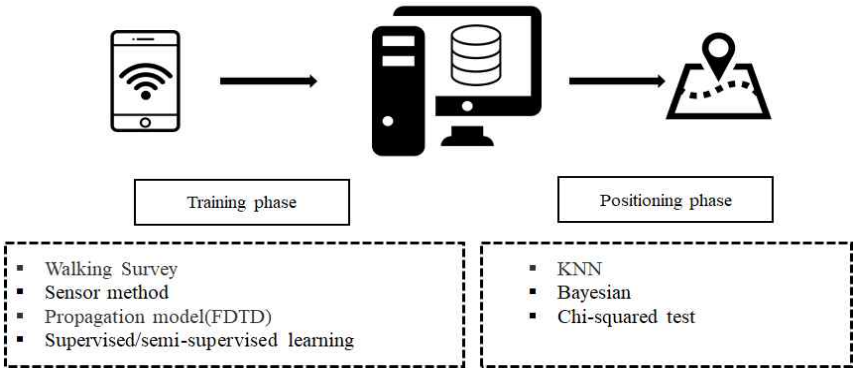

Fig. 2.6 The typical application algorithm according to the phase

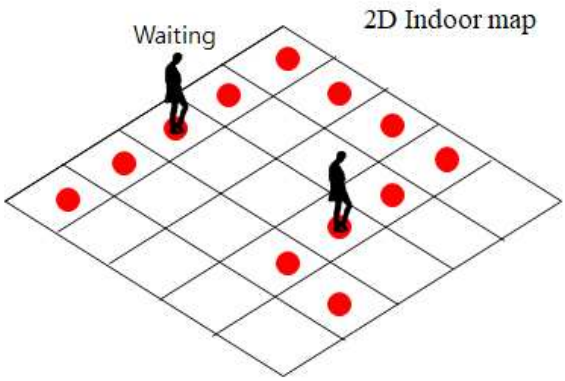

(a) Point-by-point calibration

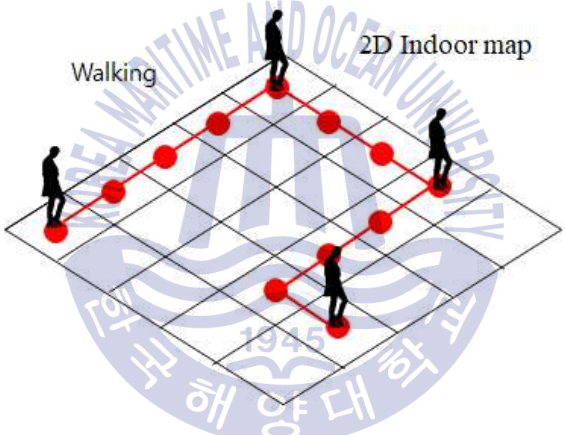

(b) Fusion sensor based classification

Fig. 2.7 The method of typical walking survey

The acquisition process of the RSSIs, which is the basic step for generating the radio map, is based on an inertial-sensor-based method [6, 26-28], a walking survey method [28], and a channel-modeling-based prediction method [29, 30], as shown in Fig. 2.6.

As shown in Fig. 2.7, the walking survey method is divided into a point-by-point calibration that concentrates signals only at reference points and

a fusion-sensor-based calibration that classifies consecutive Wi-Fi signals obtained by walking according to the reference points. Point-by-point calibration is a method of measuring RSSIs several tens of times, with enough time per reference point (indicated by a red circle). This method generates the highest time costs because all the reference points consume a certain amount of time. Nevertheless, the accuracy of the radio map is high, owing to sufficient signal collection at the reference points.

On the other hand, the fusion-sensor–based classification is a method of measuring the RSSIs of APs while moving according to a predetermined movement route by using fusion of a walking and inertial sensor. The inertial sensor is the most commonly used sensor because it is built in the smartphone. Therefore, the fusion-sensor–based calibration is less time consuming than the point-by-point calibration because it can be measured while walking through predetermined reference points. However, because of the cumulative error of the inertial sensor, generated during movement, there may be a decrease in the positioning accuracy due to a mismatch between the reference points and measurement location [31-33].

The radio map prediction based on the channel modeling extracts the radio-characteristics model of Wi-Fi and estimates the position of the user from the obstacles and distances, based on the coordinates of fixed APs.

The finite-difference-time-domain (FDTD) and log-distance path loss models are the most widely used indoor channel modeling in the fingerprint. The FDTD is widely used for modeling the radio emission characteristics of small electronic devices; however, it is necessary to specify the accurate physical coefficients for the characteristics of the surrounding medium in which

reflection and absorption of the radio occur. Therefore, a comprehensive mathematical analysis of the propagation, reflection, and absorption coefficients, and the distortions due to the arrangements of a wide variety of indoor structures such as walls and windows, is needed over a relatively large area. The Wi-Fi signals obtained for generating a radio map, using these methods, are subjected to preprocessing such as optimization and relocation.

In these pre-processes, the data are processed according to the format of the radio map suggesting the measured Wi-Fi signals, and the user finally generates the desired radio map. Here, the typical RSSI classification and optimization techniques used for processing the radio map are supervised and semi-supervised learning algorithms such as the support vector machine (SVM) or principal component analysis (PCA), and discretization and classification algorithms such as the MDLP or chi-squared test, and etc [34-36].

The SVM is an algorithm that classifies the RSSI measured by the walking survey method, according to the magnitude, and generates the radio map by matching it with the reference points. The RSSIs measured by the fusion-sensor–based classification of the walking survey are continuous, but the classification for the reference point is not clear. The SVM classifies data according to the magnitudes of the RSSIs and matches each reference point to these unclear RSSIs. This algorithmic feature is applicable to the real-time Wi-Fi signals measured from users in the positioning phase, as an algorithm that can determine positions based on the classified RSSIs [37-39].

The PCA, which is an algorithm for re-dimensioning multi-dimensional data by realigning large-sized data according to their orders of magnitude, is

widely applied for the size reduction and optimization of the radio map. The PCA used to optimize the generated radio map disassembles the APs according to the order of magnitude of the variance values when mapping the RSSIs on a single axis in the radio map. The dispersion values of each AP indicate the characteristics of each AP, and the RSSIs of the radio map can be reduced according to the number of principal components [40, 41].

As one of the discretization algorithms that can separate data into several signals, according to continuity, the MDLP is an algorithm that can simultaneously optimize and classify data. This algorithm divides the sets of RSSIs using entropy, which is a measure of disorder, for discretization [42, 43]. Entropy can express the probability that a certain value will appear in one data set, which is expressed by equation (2.3).

$$P_i = \frac{D_i}{T} \tag{2.3}$$

Where T represents the total number of data, and D_i indicates the number of times any arbitrary value has appeared. Therefore, P_i is equal to the probability that a single value will come from the entire data. According to the definition of the log function, it can be expressed by the equation given by

$$-\log_2 P_i = I(m) \tag{2.4}$$

Here, I is an information amount and m denotes an arbitrary value in the

set. When P_i=1, where the data set is constant, it can be confirmed that this data set has regularity as an amplitude of one RSSI. On the other hand, if P_i=0, it means that the value m in the data set does not exist. The amount of information of such a value can be expressed mathematically, and it is expressed by equation (2.5).

$$E = -\sum P_i \log_2 P_i \tag{2.5}$$

Here, E represents the entropy, which is the average information amount. Therefore, if the elements in the set have regularity or appear as one value, the entropy is lowered. The more irregular the data is, the more the entropy will increase. Thus, a set, which explicitly presents the distinction of the measured elements in a continuous time order, indicates that the number of subsets divided by the discretization increases, and that the values of the subset are clearly different from each other. The MDLP with these properties is expressed by equation (2.6).

$$MDLP(X,T,S) = \frac{|S_1|}{|S|}E(|S_1|) + \frac{|S_2|}{|S|}E(|S_2|) \tag{2.6}$$

Here, S means the whole data in the set, T means the dividing point for the condition X, and S_1 and S_2 indicate two subsets of S divided by T. Therefore, as the number of subsets due to the discretization of the set increases, it means that the reference points are properly classified automatically. Based on this, if MDLP is applied to the relationship of AP

aggregates rather than to a single set, the APs can be removed by using the property that signals that should have similar distributions of elements are not divided. Since the MDLP itself splits the continuous data, there is no numerical value to check the result separately. Therefore, to verify the performance of the MDLP, the information gain (IG), which indicates the amount of entropy applied to determine the continuity of data after applying the MDLP.

In this case, the IG values of the RSSI set, which clearly distinguish the data, appear larger and the APs that the RSSIs find difficult to distinguish are converged to 0 by the IG. In other words, the RSSI set of APs with a value of 0 can be defined as an AP that can cause confusion in positioning because the measured RSSI results at the different reference points are similar [44].

Fig. 2.8 shows the IG values obtained as a result of applying MDLP and IG to the RSSI aggregates of each AP. The x-axis represents the SSID of each AP and the y-axis represents the value obtained by applying the MDLP and IG. As described above, the APs with an IG value of 0 indicate that it is difficult to distinguish the measured RSSIs according to the reference points. Especially, Wi-Fi signals have high standard deviations because they have large variations of RSSIs even at one reference point. Therefore, this removal of APs is effective in reducing the size of the radio map or increasing the iteration speed.

The class-attribute interdependency maximization (CAIM) and class-attribute contingency coefficient (CACC) are discretization algorithms similar to the MDLP. Unlike the MDLP based on entropy, both these algorithms partition data based on probability-based interdependencies. Therefore, since these algorithms

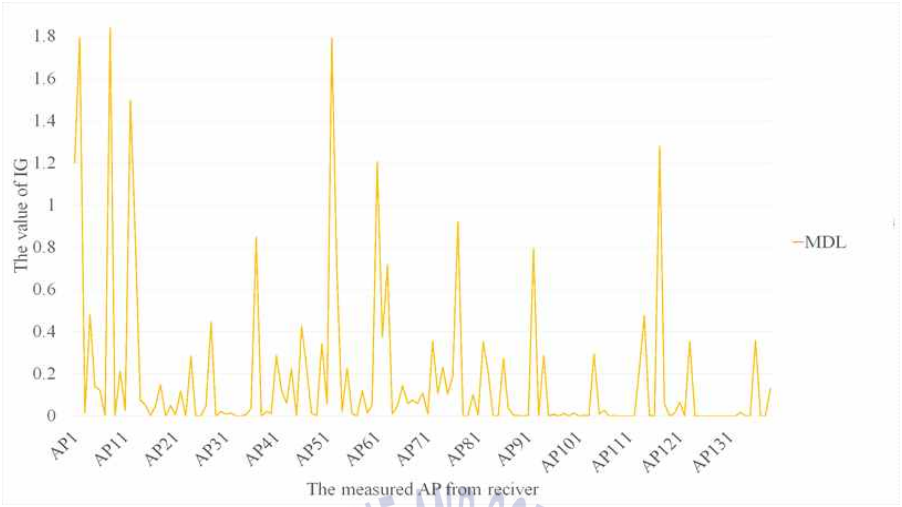

Fig. 2.8 The visualization of MDLP via IG

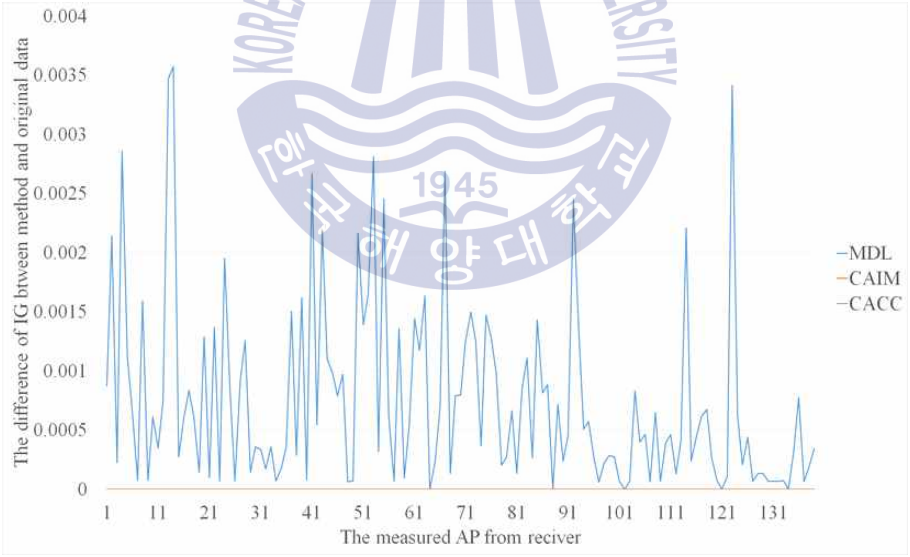

Fig. 2.9 The performance comparison of MDLP, CAIM, and CACC

do not use the entropy in the computation process, an entropy derivation process is needed to apply the IG; the discretization performance is also lower

than that of the MDLP.

Fig. 2.9 shows the results of an experiment comparing the performance of MDLP, CAIM, and CACC. The x-axis is the SSID of the AP and the y-axis is the difference value of the IG of the MDLP with respect to the IGs of CAIM and CACC. Since they are derived from the same algorithm, the discretization performances of CAIM and CACC are similar; the IG results of both algorithms are also the same. Among the three algorithms, the discretization of MDLP is the best, but the difference is very small. To distinguish it, the y-axis is expressed as the difference by setting the IGs of CAIM and CACC to the reference value of zero. The size of the y-axis is very fine, but these results have a large impact on the ability of removing the APs.

2.2 Unsupervised Learning

2.2.1 Neural Network

Recently, research on neural networks has been increasing, and machine learning algorithms are fundamentally classified into neural network-based and non-neural network-based learning algorithms.

SVM and PCA, which are non-neural network-based supervised and semi-supervised learning algorithms, can be used as positioning and RSSI classification and optimization for the fingerprint. Because these algorithms do not use a neural network, their computation complexity is relatively low. However, their application scope is somewhat limited.

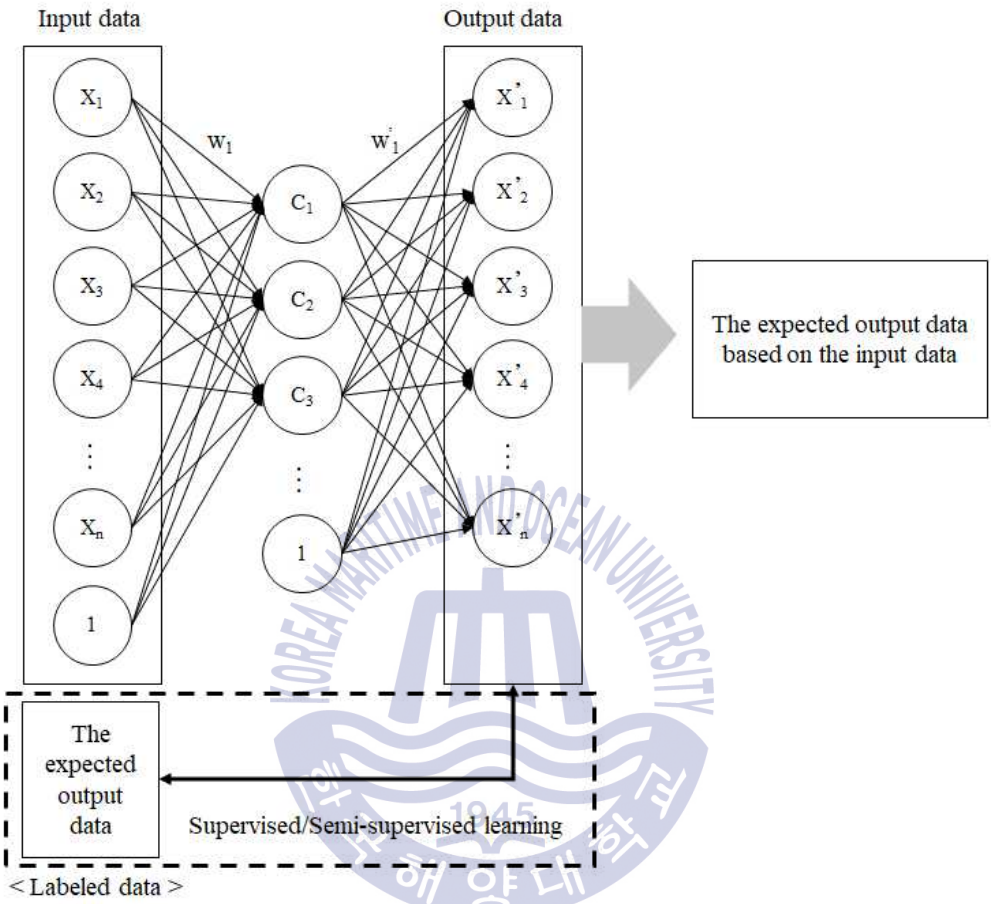

Fig. 2.10 The network structure of supervised/semi-supervised learning

As shown in Fig. 2.10, neural network-based supervised and semi-supervised learning algorithms interpret features through interconnections of the hidden layer between the input and output data. Neural network algorithms (e.g., convolutional neural networks (CNN) and recurrent neural networks (RNN)) use supervised and semi-supervised learning from the endpoints, based on the correct answer data, to update the connected weights (W_1, W_1') around the hidden layer. Thus, these algorithms require minimum training data and

labeling with correct answer data.

Labeling refers to the process of inducing the output of the desired data by allowing the user to compare expected output data directly to trained output data. This is identical to the concept of passive clustering. Data created through this process is called “labeled data” and is an essential process for acquiring a properly trained model for supervised and semi-supervised learning. Therefore, learning performance is determined by the quality of the label, the size of training data, and the training volume. It is applied to regression, classification, prediction, etc., depending on the method of use [45–48].

Table 2.2 shows the result of comparing the characteristics by the learning

Table 2.2 The the result of comparing the characteristics by the learning algorithm type

Classification	Supervised learning	Semi-supervised learning	Unsupervised learning
Organization of data sets	Labeled data	Labeled data, Raw data	Raw data
Algorithms	KNN, SVM, Linear model, Neural networks	Label propagation, Neural networks	PCA, Autoencoder, K-means, DBSCAN
Application	Regression, Classification, Prediction	Regression, Classification, Prediction	Clustering, Prediction, Feature extraction

algorithm type. While developing and training a learning algorithm, the labeling process consumes a considerable cost and lowers the accuracy of the algorithm, making it dependent on the initial design. By contrast, unsupervised learning has the advantage of not requiring labeled data. Thus, it learns the original data as input data with no separate processing of features to derive the desired result. Therefore, when applying supervised and semi-supervised learning to a radio map, must be directly measured at the same location and input as labeled data. Furthermore, because the distribution of RSSIs can be greatly distorted and unclear, depending on the indoor structures and radio environment, there is limited scope for improving the label quality in order to enhance the accuracy of the learning algorithm. Therefore, the proposed

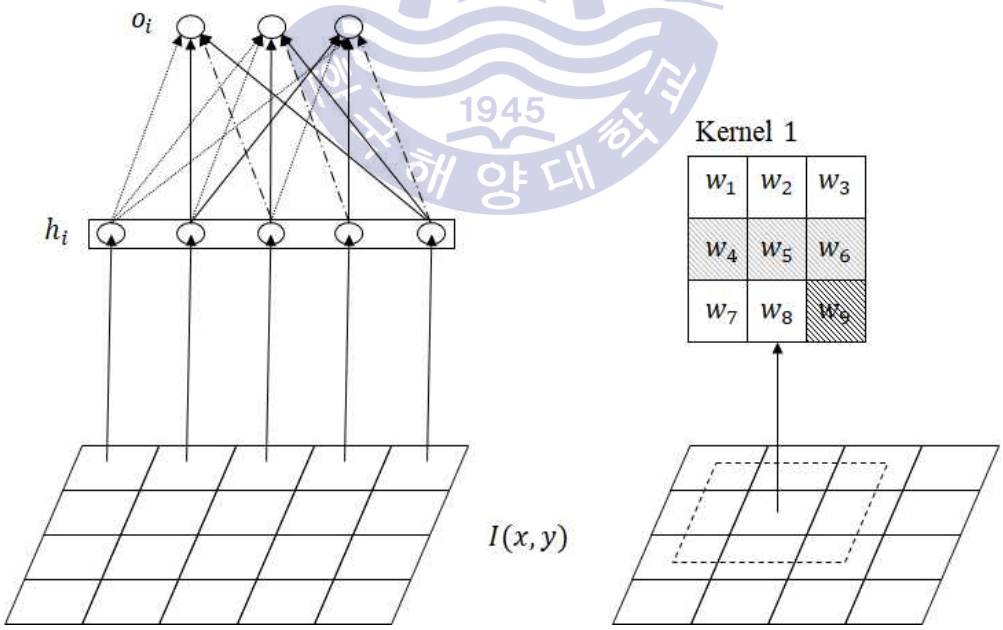

Fig. 2.11 The structure of dense layer and kernel configuration

algorithm adopts unsupervised learning, which does not require unsupervised learning, which does not require direct measurement. Neural network-based machine learning algorithms are designed based on a deep learning structure, stacked with multi-layers. Each layer can be designed to output the user specified results.

Generally, neural networks have a dense network structure in which all input and output nodes are interconnected, as shown in Fig. 2.11. Here, $I(x,y)$ represents the 2-D input data consisting of h_i, which is the feature vector set of the hidden layer and o_i, which is the output feature vector set calculated through the multiplication operation of the weight group. A group of independent weights is a "kernel". In the case of DenseNet, an entire layer is one kernel, because all weights are independent. Because this layer can perform

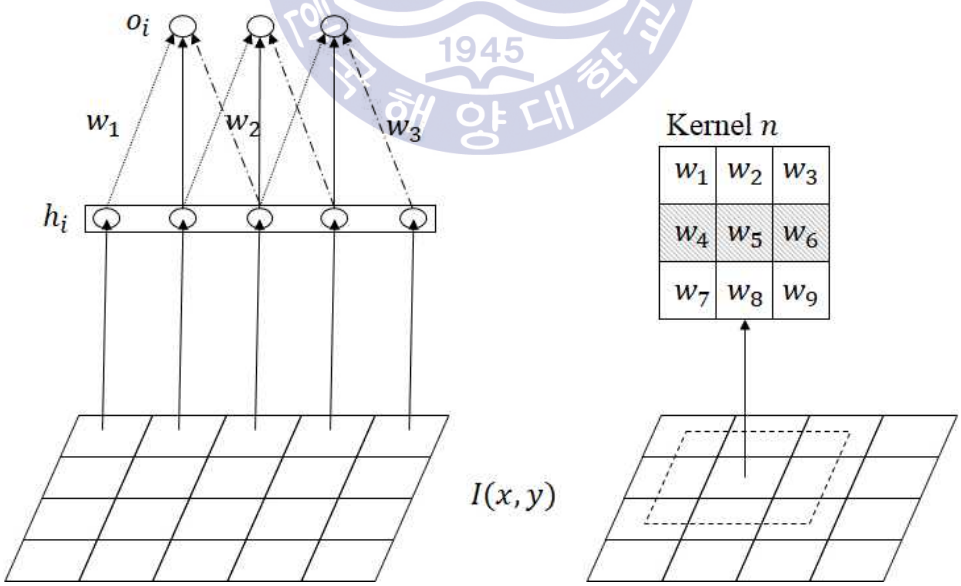

Fig. 2.12 The structure of CNN layer and kernel configuration

all types of operations, it also has the fundamental disadvantage of being unable to extract widely used layers, local characteristics, and biased characteristics. To overcome this disadvantage, the CNN, which is often used for images, shares the weights without making them independent in one layer.

Fig. 2.12 shows the structure of CNN layer and kernel configuration. Here, $I(x,y)$, h_i, and o_i are the input data, the feature vectors of the hidden layer, and the output layer, respectively. Furthermore, the solid, dotted, and double-dotted arrows denote connections of w_1, w_2 and w_3, which are shared amongst the nodes. The CNN layer, which has a group of non-independent weights, can have multiple small weight groups, unlike the DenseNet, and thus can have diversity of expressions with n kernels expressing various characteristics.

2.2.2 Autoencoder

Neural networks are classified into backward and forward types, depending on the weight (W) update method. The backward type represents supervised learning in which the relationship between input and output is functionalized with all input and output data acquired as training data. Here, training data is labeled data, because the label, or the result of the classifier, is input with the data. For most learning algorithms, it is critical to acquire a large quantity of high quality data before learning, because the quantity and quality have a significant effect on performance.

However, because the labeled data are mainly created manually, it is time consuming and difficult to acquire a large quantity of data consistently.

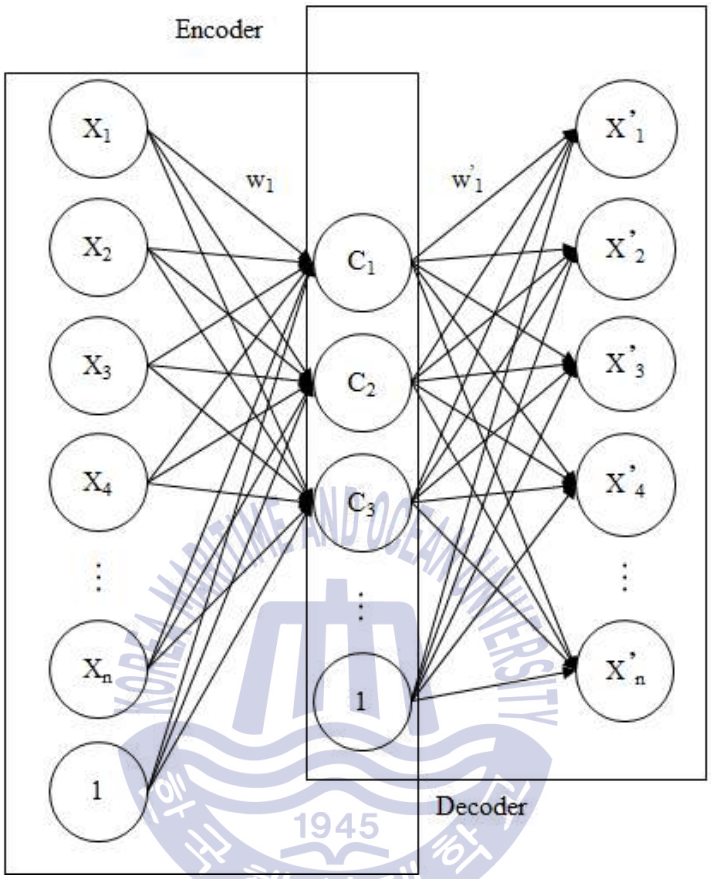

Fig. 2.13 The structure of conventional autoencoder

Therefore, researches are being conducted to reduce labeled data by using an unsupervised algorithm or by improving a supervised learning algorithm.

As a representative example, to avoid using labeled data, an autoencoder performs labeling by itself based on the probability distribution of features by simply using the input data. It copies the learned training data to new output data. In the image processing field, this technology is applied for the creation and restoration of images as an image reproduction algorithm.

Fig. 2.13 shows the structure of the most basic autoencoder. Using training data consisting of input data and one datum having the value of 1, the autoencoder encodes signals feature vector C of the deterministic function type according to each feature. Then it carries out data restoration by decoding it again.

Additionally, the input value, 1, is a bias to maximize the approximation by quickly adjusting the characteristic curve of probability distribution to derive C, based on the training data. The operation process of each input value can be shortened by adjusting this value.

The input function, X_n, can be expressed as follows with weight value (W) and bias (b):

$$C = \sigma(Wx + b) \tag{2.7}$$

where W is the weight value according to each input data, x, in the feature vector function, C, and b is the bias of data. This function is used to recreate output from the decoder, as shown in equation (2.8). As the amount of training data increases, W and b are trained as a function with a more accurate output value.

$$y = f(c) = \sigma(W'x + b') \tag{2.8}$$

Because this cloned data do not require any featured function setting or labeled data, and the input and output data are always identical, the autoencoder cannot use complex input data, and the scope of its application

is also limited [49–51]. To improve the performance of this autoencoder, recent researches apply a deep autoencoder by dividing it into encoder and decoder and reconstructing it into deep neural networks performing the same role.

2.2.3 Generative Adversarial Network

A neural network based on probability distribution is a method of weighted learning that maximizes the log-likelihood. Generally, numerous approximations are required for the log-likelihood gradient. Thus, a generative machine is applied, which can derive results simply through a pre-trained machine. The back-propagation, which is a core algorithm of the supervised learning based neural networks, definitely requires ground truth. Thus, as it is inappropriate for the generative model with no training data, which is the objective of learning. Past researches applied such methods to an autoencoder, which uses input data as training data. However, GAN is recently proposed to improve prediction performance through mutual learning of the training model.

GAN, a generative machine, was developed as a technology to generate images. It is a network that creates the learning function while increasing accuracy by itself via competition between the CNN-based “generator,” which creates images, and the CNN-based “discriminator,” which compares the actual and created images.

Fig. 2.14 shows the structure of this network. For an initial training, the generator, which receives Gaussian noise as input, generates fake data per the predefined pixel size. The discriminator compares the real data to be trained

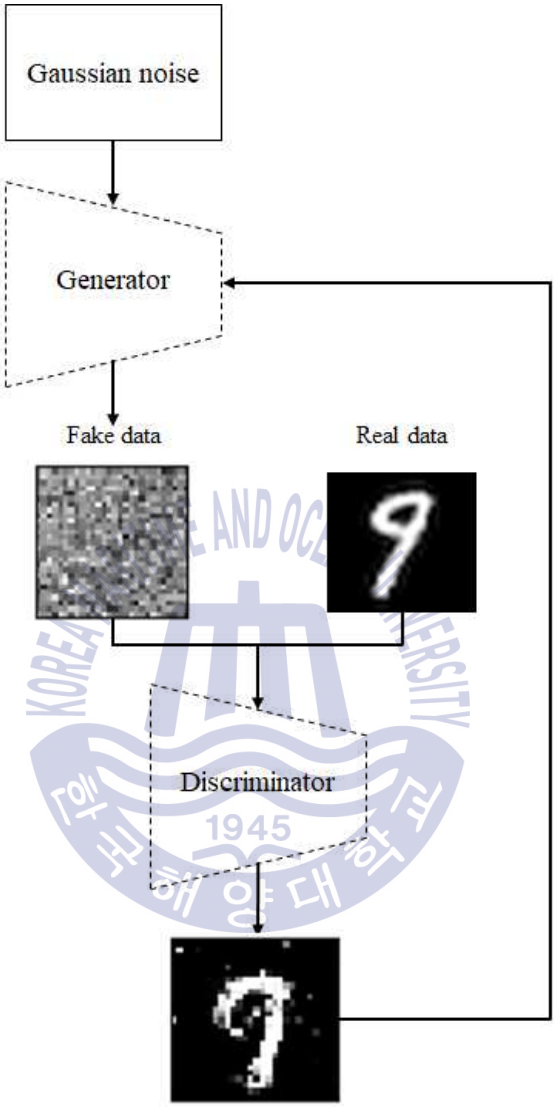

Fig. 2.14 The structure of conventional GAN

with the fake data and trains only the matching pixels by comparing them. Simultaneously, the generator receives only the information of unmatched pixels from the discriminator, and the recreation process of fake data is performed repeatedly. This competition process (i.e., minimax game) can be

expressed as the function, $V(D, G)$, as follows [52].

$$\min_G \max_D V(D, G) = \mathrm{E}_{x \sim p_{data}(x)}[\log D(x)] + \mathrm{E}_{z \sim p_z(z)}[\log(1 - D(G(z)))] \quad (2.8)$$

Where, for the generator to learn the distribution curve, K_g, of input data, x, the derivative function (fake data), G, of the first multi-layer perceptron having the Gaussian noise $N(z)$ as general noise data. Parameter, θ_g, is expressed as $G(z;\theta_g)$ in the data space. Here, when the second multi-layer perceptron outputs a single scalar, expressed as $D(x;\theta_d)$, $D(x)$ is the probability of appearing in input, x, rather than in the distribution curve, K_g. D is trained to maximize the probability of the real data, and fake data, G, is used to create the correct label. Simultaneously, G is trained to minimize $\log(1 - D(G(z)))$.

The learning process of this operation is expressed in Fig. 2.15. The data, $x = G(z)$, are the results of projecting the input noise, z, by the generator. (a) represents the data distribution status prior to initial learning. The random green G function generates values in the shape of a Gaussian distribution, and the blue D function represents a random curve, because it occurs before distinguishing the blue D from the actual data. When learning begins, as shown in (b), the discriminator, D, is generated as a sigmoid function curve, because it distinguishes the true and false data. In step (c), where all signals are determined to be true, and the generator generates actual signals, D appears as a straight line, because it only has true values. When the generator becomes a generative machine that generates data close to the real

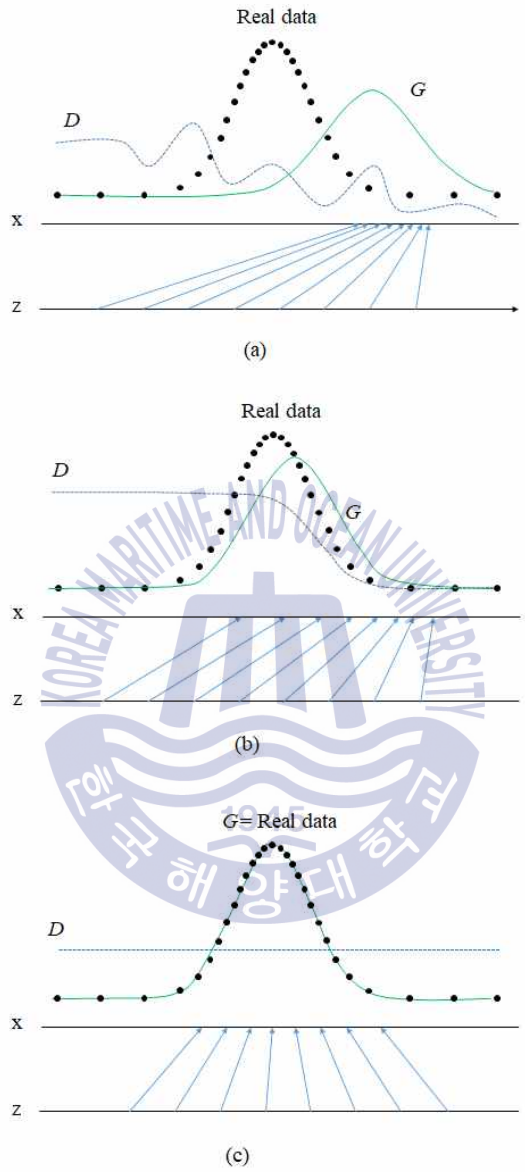

Fig. 2.15 The data learning process by GAN

data through this process, the discriminator is finally removed to use this learning machine, and it is applied as shown in Fig. 2.16. Here, the learned

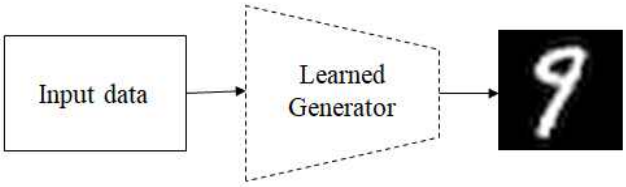

Fig. 2.16 The application of learned generator

generator is a network that generates the number 9. When a generative machine consisting of these multiple generators is composed, a new network that can distinguish and create more various images from the input data can be created [53].

Chapter 3 Proposed Fingerprint System

3.1 Unsupervised Dual Radio Mapping Algorithm

In this chapter, the proposed unsupervised learning-based fingerprint system, which leverages the proposed UDRM algorithm in the training phase

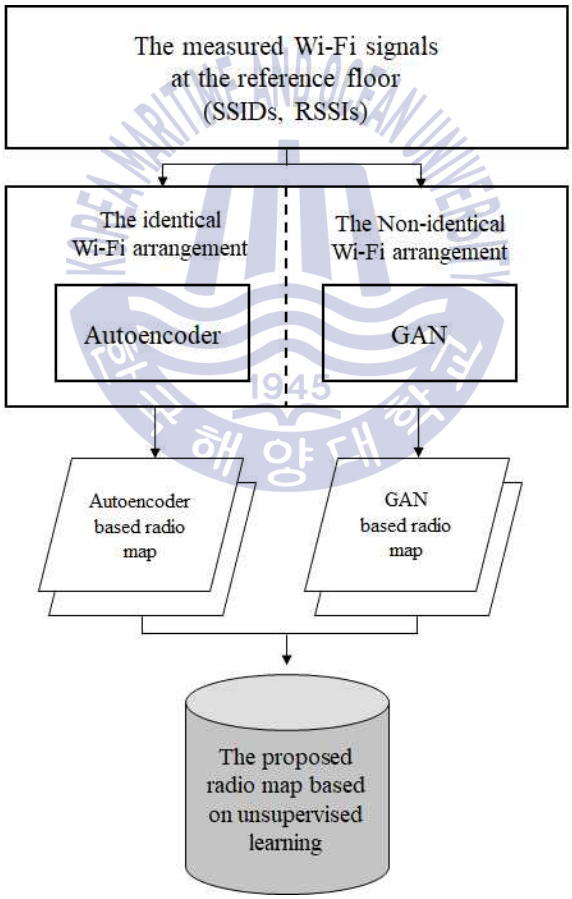

Fig. 3.1 The structure of proposed UDRM algorithm in the training phase

and the proposed MDLP-based RMF algorithm in the positioning phase, is described in detail.

Fig. 3.1 shows the structure of the proposed UDRM algorithm in the training phase. The proposed UDRM algorithm, based on the autoencoder and the GAN described in chapter 2, is applied two modified algorithms that generate a radio map according to indoor structures and measured Wi-Fi data within the reference floor. First, to minimum learning, the proposed algorithm measures the SSID and relative RSSI according to a set reference point on the reference floor of the building where user locations can be recognized. Based on the measured Wi-Fi, a real radio map for learning is preferentially generated on the reference floor. The RSSIs in the radio map only measures fixed AP that do not change. Generally, the main APs installed in a building cover the entire area and are always fixed and operated. Additionally, the coordinates of the APs are easily obtained via indoor 2-D maps.

After that, based upon the floor where the radio map is to be generated, the autoencoder or the GAN is selectively applied according to the indoor map and the coordinates of APs on other floors. If the 2-D maps and the coordinates of APs on new floors exists, the proposed algorithm can be applied automatically. To reduce iteratively learning-time and to ensure positioning accuracy in the positioning phase, the initially measured APs (i.e., learning objects) are selected only for the main APs of Wi-Fi having an extremely low probability of being removed.

The modified autoencoder in the proposed UDRM algorithm is then applied to other floors having nearly the same indoor structures and the coordinates of APs, like the reference floor.

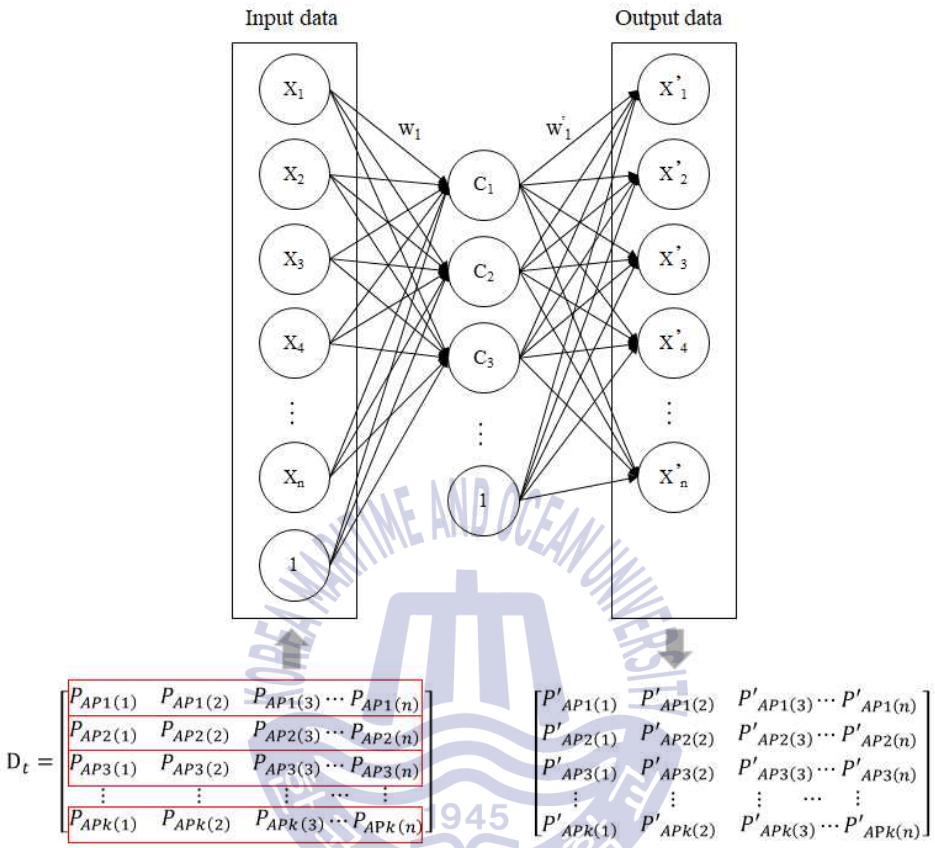

Fig. 3.2 The type of input/output data of modified autoencoder

Fig. 3.2 shows the structure and input/output data of the modified autoencoder for applying the fingerprint. D_t is a set of RSSIs measured from the walking survey. The RSSIs measured on the reference floor are learned to generate the RSSIs on the other floors. The form of input to the autoencoder is shown in equation (3.1).

$$AP^i = [AP_1^i, AP_2^i, AP_3^i, ..., AP_R^i]^T \tag{3.1}$$

where, R is the location of the reference point, and AP^i is the set of RSSIs according to the reference point of the i-th AP. When AP^i is learned as input data, their RSSI distribution curves are obtained for the entire radio map. As the amount of iterative learning for the same AP gradually increases, so does the accuracy of the distribution curve. Even if the positions of the reference points change, the prediction accuracy of RSSI between a receiver and a transmitter increases.

Fig. 3.3 shows the comparison of the autoencoder performance according to the learning iterations. (a) is the result of the replicated signal with a small amount of learning, and (c) is the result of the replicated signal when the amount of learning is sufficient. The black dots represent the data learned from the input data, and the green line represents the result of the prediction data between the black dots. Thus, with much iterative learning, (c) can predict the signals more accurately than (a). This algorithmic feature is advantageous for the replication of signals when the same data is learned, but can be advantageous for prediction when intermittent signals such as Wi-Fi,

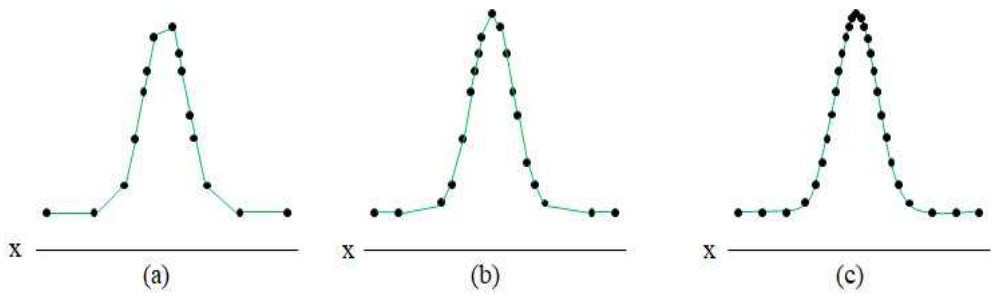

Fig. 3.3 The performance of autoencoder according to iterations

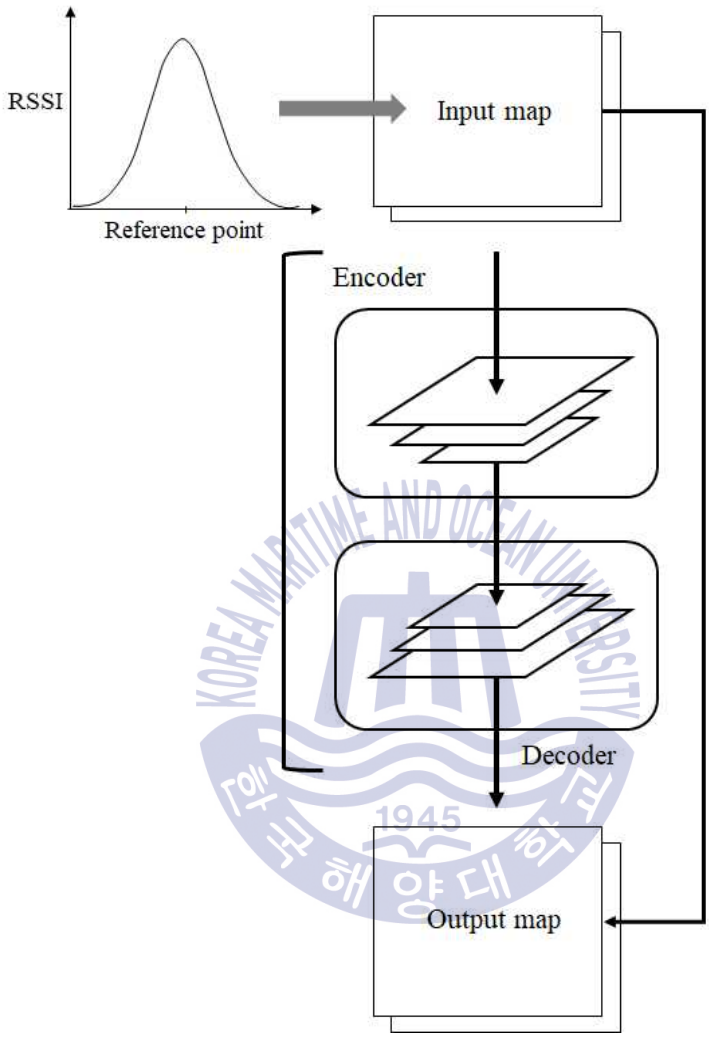

Fig. 3.4 The learning of the modified autoencoder

are learned. Therefore, the Wi-Fi RSSIs measured is inputted the proposed unsupervised learning based on autoencoder without any additional processing and replicate their signals. In addition, if only the coordinates of APs are added as input data with the measured RSSIs of APs, it is robust to the reference points change, because the RSSIs between the reference points are

predicted to high accuracy. Therefore, the radio map is predicted and generated with the proposed algorithm on the other floors of the same structure. Therefore, the radio map is predicted and generated by the proposed algorithm on the other floors of the same structure.

Fig. 3.4 shows the structure of an modified autoencoder that maps input RSSIs to the 2-D map and uses the data as input for the autoencoder to learn the characteristics of the RSSIs emitted from the Wi-Fi APs on the other floors of the same structure. The inputted radio map, which is measured on the reference floor, is updated by comparing the weight of the autoencoder against the generated radio map, and the autoencoder consists of encoders and decoders.

In the modified autoencoder, the encoders and decoders are designed symmetrically to compress and expand the types of input data. Because the input data is output as RSSI for each referenced position, (Fig. 3.4), it is necessary to combine it with real 2-D maps. During the real prediction process, the measured RSSIs are not used as input data, because a new floor is an unmeasured area. Thus, the coordinates of the APs on the new floors should be input.

Fig. 3.5 shows the prediction process of the modified autoencoder, which belongs to a generation model that inputs similar data or noise, and outputs the result using the same distribution as the input data. The measured RSSIs on the reference floor and coordinates of APs on the other floor are input simultaneously. The dotted-line graph atop the Fig. 3.5 indicate a linearly approximated Wi-Fi signal attenuation for coordinates of AP. As in the learning process, the estimated RSSI value is mapped to the 2-D map to

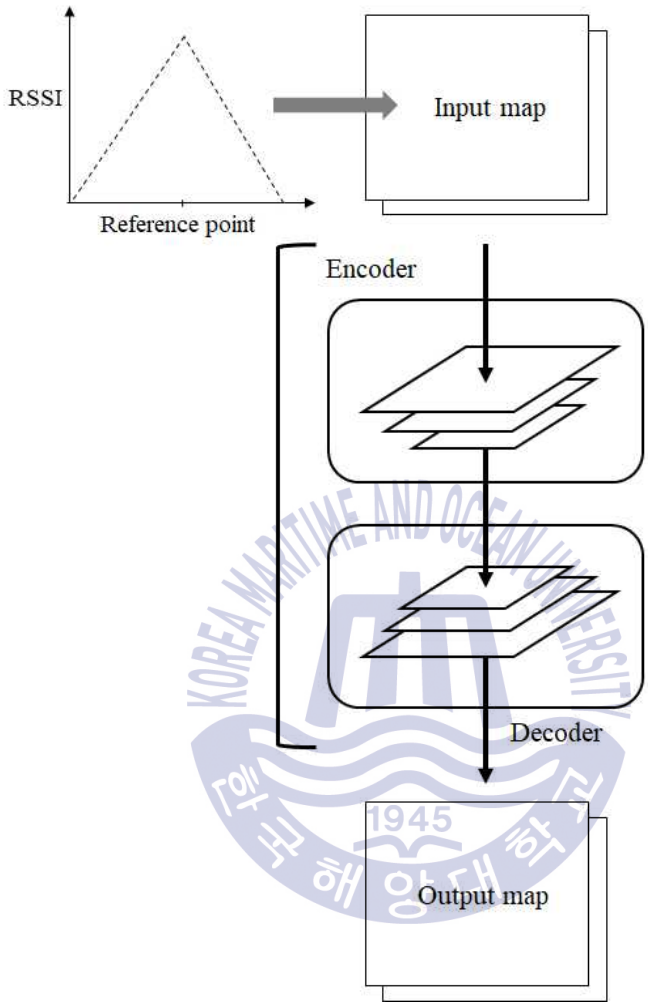

Fig. 3.5 The prediction of the modified autoencoder

generate input data, and the predicted radio map is generated with the learned algorithm. The generated radio map of each AP is predicted considering the coordinates of the installed APs on the new floors, assuming the same structure as the measured reference floor and the learned indoor structures. In case the floors with different indoor structures, the modified GAN is applied

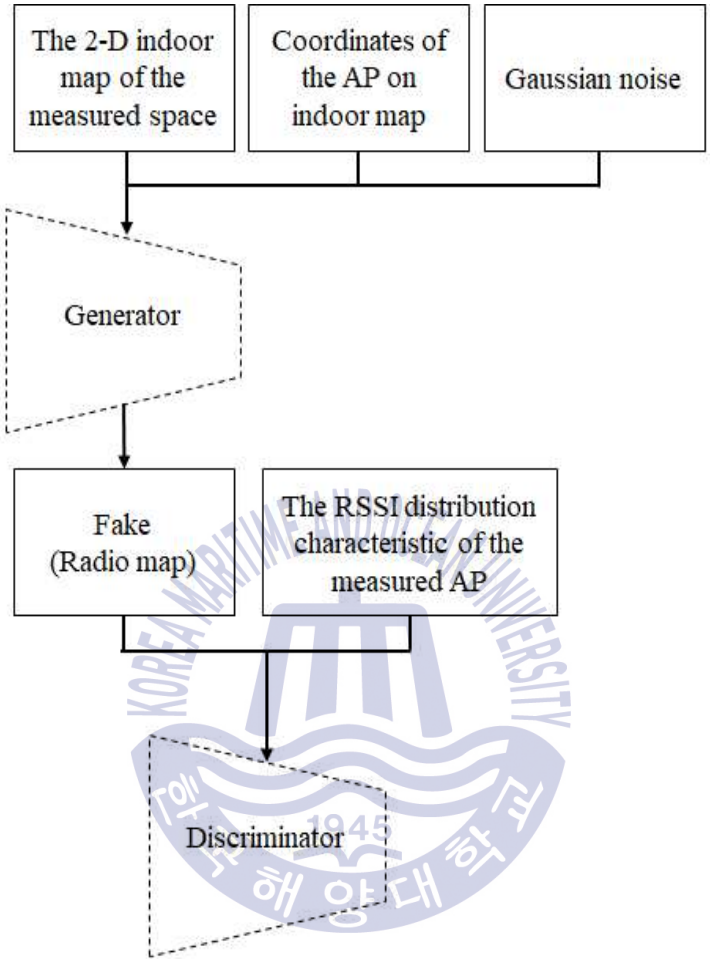

Fig. 3.6 The structure of the modified GAN

instead of the modified autoencoder. The modified GAN-based radio map generation algorithm can be applied to indoor environments where the reflection and refraction characteristics of the radio are the same, even if the installed coordinates of the APs and indoor structures are different.

Fig. 3.6 shows the structure of the proposed GAN. Unlike the general GAN structure, where only Gaussian noise is input to the generator, the

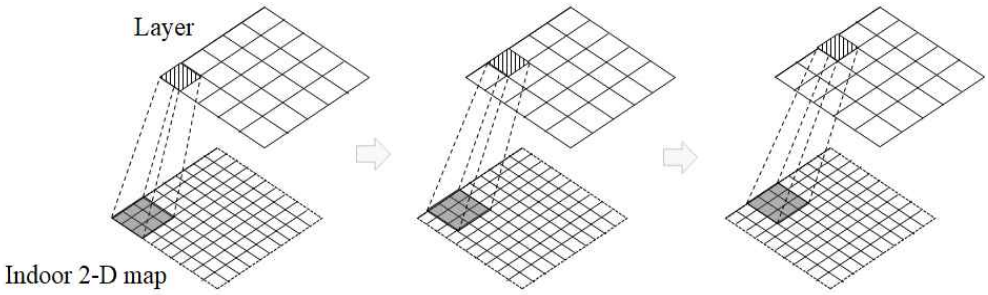

Fig. 3.7 The learning principle of the discriminator

modified GAN is inputted Gaussian noise as initial data along with a 2-D map and coordinates of APs on the new floors. The 2-D map is the input data for effective radio map-matching, because it grasps the indoor structures of the floors through the measured radio map on the reference floor.

Thus, the coordinates of APs are essential data for generating the radio map at the correct position and predicting the RSSIs. An initially non-learned generator creates random RSSI distributions from the Wi-Fi signals generated by Gaussian noise through the input 2-D map and coordinates of APs.

The fake radio map, which is generated by the Gaussian noise, divides the real measured RSSI on the reference floor and each generated RSSI by the discriminator into true or false per a pixel in the map.

Fig. 3.7 shows the learning process of the CNN-based radio map, which is the basic structure of the discriminator that classifies the generated radio map into true and false. The discriminator is learned the data of the fake radio map which is combined the 2-D map and the coordinates APs. The fake radio map is compared to the real radio map, and the discriminator is only given the false RSSI pixels in the fake radio map as the input data of

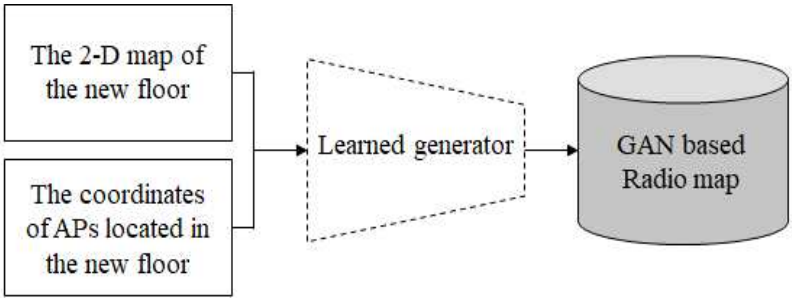

Fig. 3.8 The application method of the modified learned generator

the generator for learning. This process re-predicts the accurate radio map via iterative learning. The kernel can freely acquire information of the combined radio map according to the shape of the sample, and it can predict the partial 2-D map and RSSI distributions of various kernels simultaneously using learning generator in GAN. The kernel applied in the proposed algorithm learns from a wide range of pixel sizes and shapes: from 2x1 to the entire map size. If enough generation data is learned through iterative learning, it becomes a radio map generator, which stores the APs and indoor environments of the learned building into the various kernel forms.

Fig. 3.8 shows the radio map generation by the learned generator of GAN of new floors. The learned generator combines the various learned types of kernels and predicts the RSSI distributions using the 2-D map and the coordinates of the APs on the floors that are different. Thus, the proposed radio map generated by the combined autoencoder and GAN maps, so that the RSSI distributions of all floors and areas are generated without complex measurement processes in a new area.

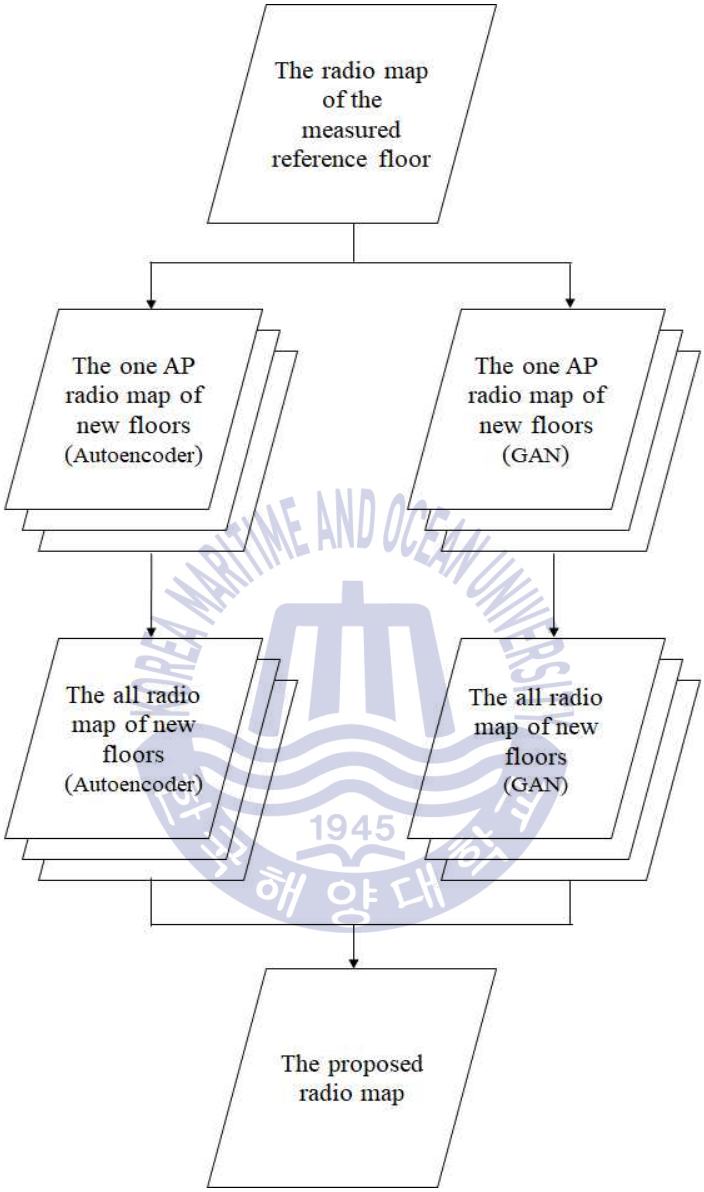

Fig. 3.9 The order of construction the entire radio map

Fig. 3.9 shows the process of combining the generated radio map into an entire radio map. The RSSI distributions, according to the transmission power

of AP, are predicted and combined to generate a radio map of all floors. Because the modified autoencoder and GAN-based unsupervised learning algorithms are designed around networks like CNN and RNN, they respond flexibly to data input for iterative learning. In this process, over-fitting happens when an algorithm learns 100 % of the detail and noise from the training data such that it negatively impacts the performance of the model. Often, the noises or random fluctuations of the training data are picked up and learned as concepts by the model. Therefore, networks that are robust to this phenomenon have prediction errors in the range of 5 to 10 %. However, prediction errors of 10 % or more begin to deteriorate learning performance. It is necessary to the stabilize the prediction accuracy through sufficient measurement data and iterative learning.

3.2 MDLP-based Radio Map Feedback Algorithm

The generated radio maps for each floor, using the proposed autoencoder and GAN, do not measure or predict high-mobility APs, thus reducing time-cost and workloads for RSSI measurement. Therefore, additional updating of individual APs is required to improve positioning accuracy. To accomplish this, an MDLP-based RMF algorithm is proposed, which can update during positioning using the generated radio map of the UDRM.

Fig. 3.10 shows the structure of the proposed algorithm in the positioning phase. To recognize user locations through the radio map, it is essential thatthe users have smart devices capable of measuring Wi-Fi. When the radio map is acquired through this device in real-time, the radio map based on

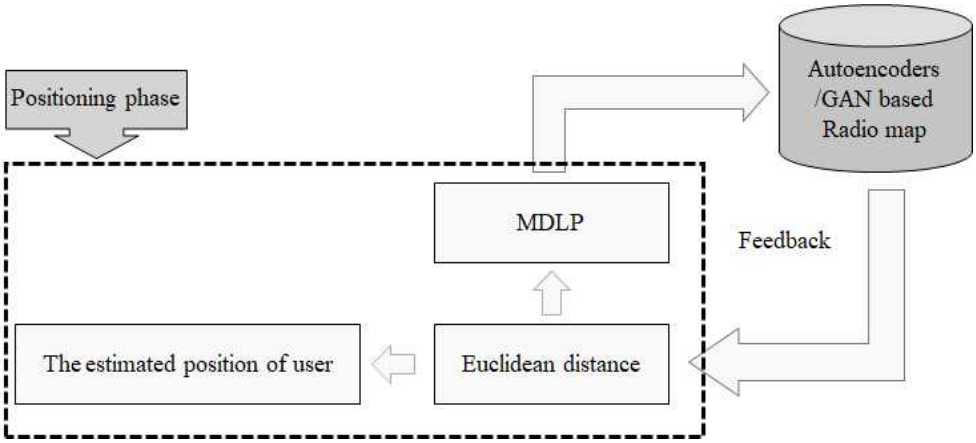

Fig. 3.10 The proposed flowchart of the positioning phase

the UDRM and the measured APs signals are compared by the euclidean distance algorithm of equation (2.2). Through this operation, the coordinates of the reference points having the highest similarity are determined to be the user locations.

Whereas the above-described process occurs in the conventional positioning phase, the proposed MDLP-based RMF algorithm optimizes and updates the new APs that is not present in the radio map during the calculation using the euclidean distance algorithm. This method improves the performance of positioning by filtering unnecessary AP signals and automatically reducing a dimension of the radio map in the area where the number of users is many and the density of Wi-Fi APs is high.

The measured Wi-Fi signals in real-time are able to positioning and compare RSSIs of the radio map. Also, they are arranged in the form of the proposed radio map according to their measured locations. It is even possible to input them into the UDRM-based radio map. However, if all measured APs

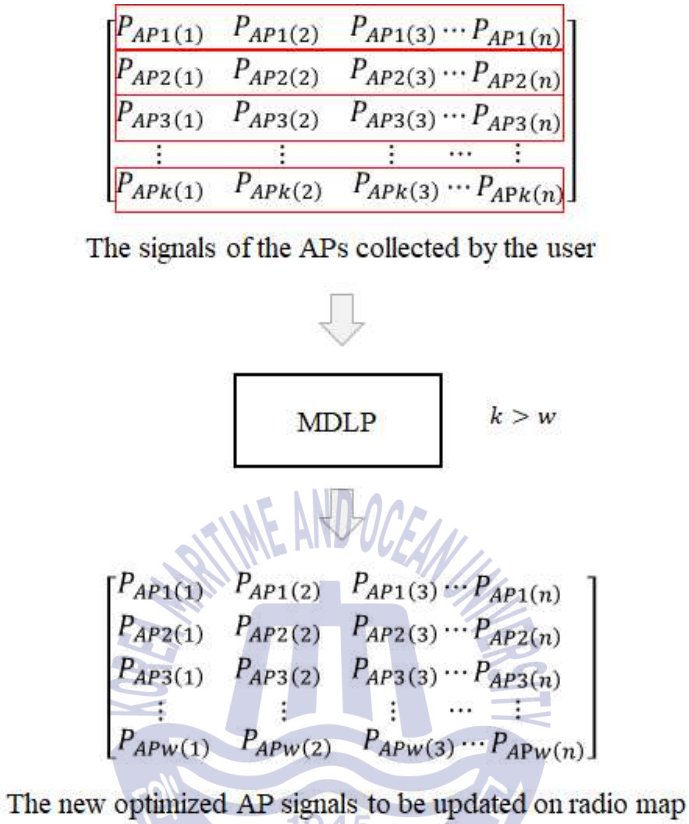

Fig. 3.11 The calculation method and output of MDLP

are input, as APs are newly created or discovered, the radio map increases, causing the operation speed to slow.

Therefore, the MDLP-based RMF algorithm should remove unnecessary APs and update the map, as shown in Fig. 3.11. Input data consists of a set of red rectangles, which are separated into several subsets via discretization of the MDLP operations performed. If the number of disjoint subsets is smaller than the reference point of the corresponding layer, the entire set of measured RSSIs can be determined to be APs that cannot distinguish RSSIs

from each reference point.

Unlike the existing method that discriminates and processes a set of continuous RSSIs measured at one AP, the proposed algorithm grasps the signal distribution characteristics among APs and obtains a plurality of them, having substantially the same signal characteristics according to the reference points, as one AP to reduce the radio map.

APs with similar signal characteristics have a very small influence on positioning, but they increase the amount of computation and the size of the radio map. The conventional MDLP algorithm cannot numerically express the degree of signal separation according to the signal reference points. So, after applying the MDLP, the proposed algorithm performs the IG operation to quantify it. The data characteristics of the quantified AP numerically represent the similarity between the different AP signals, so that only those with the best classification among the signals of similar distribution remain. Thus, each AP can visually confirm the RSSIs distinguishing ability according to the reference points and can manage the Wi-Fi signal strictly through that threshold. Therefore, the proposed MDLP-based RMF algorithm is designed to update and optimize collected Wi-Fi signals simultaneously with positioning.

Chapter 4 Experiment and Result

4.1 Experimental Environment and Configuration

To verify the performance of the proposed UDRM algorithm and MDLP-based RMF algorithm, an experimental area was selected at the College of Engineering, No. 1 Building, Korea Maritime and Ocean University, as shown in Fig. 4.1 and Fig. 4.2 The first floor, which was difficult to positioning, was excluded from the experimental area, owing to the low number of APs. Because the 2nd, 3rd, and 4th floors have the same structure, a radio map could be generated through a modified autoencoder, and a modified GAN could be applied to the 5th floor: a different indoor structure.

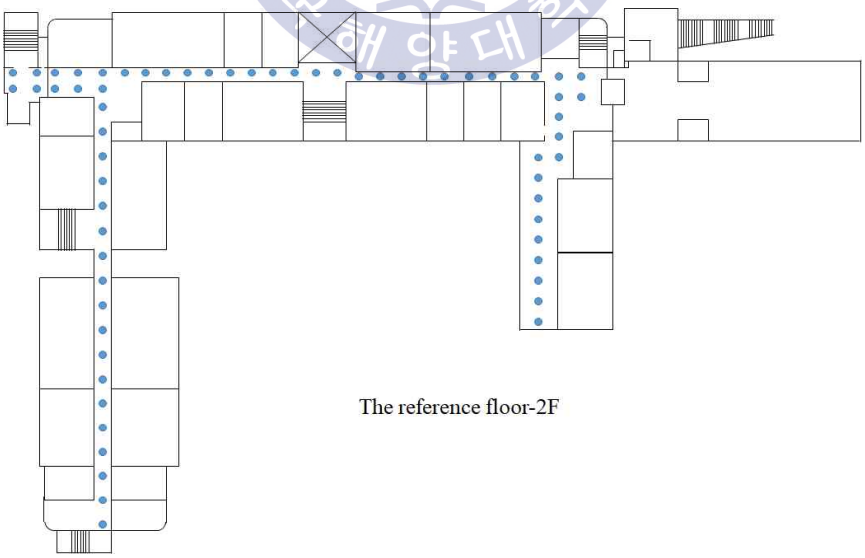

Fig. 4.1 The structure of reference floor

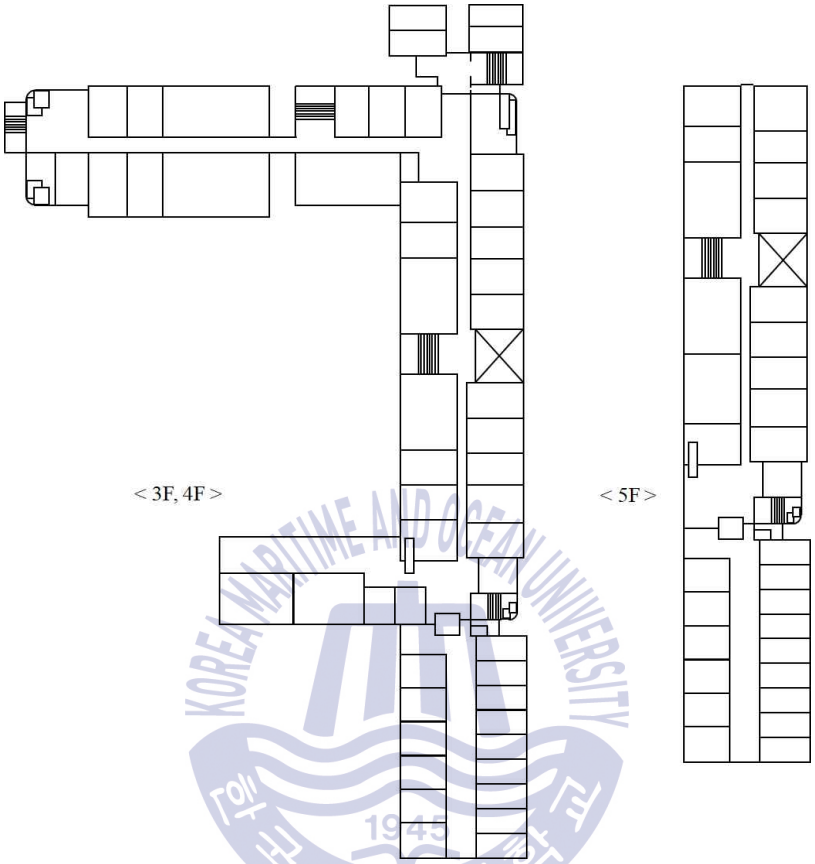

Fig. 4.2 The structure of experimental floor

The 2nd floor, where APs were sufficiently measured, was set as a reference floor for obtaining real RSSIs for learning. RSSIs were measured at each reference point through the walking survey. The RSSIs were measured using point-by-point calibration to collect the accurate RSSIs and to compare the proposed algorithm. In this process, 63 reference points were set to generate a radio map for learning, and 284 AP signals were measured along the entire floors. In the training phase, because the personal APs could easily change via generation and movement, only the public APs were measured on

(a) Android-based Wi-Fi app (b) Management server of radio map (MYSQL)

Fig. 4.3 The produced program for operating the proposed algorithm

entire floors. Personal APs omitted in the training phase could be updated through the modified MDLP in the positioning phase.

As shown in Fig. 4.3, an Android-based measurement app was created using a smartphone to measure RSSIs throughout the walking survey. The measurement items were SSIDs and RSSIs, and the generated radio map was used MySQL, allowing management of the radio map in real-time. The modified autoencoder applied the measurement data as input data without pre-processing. Thus, it directly transmitted the collected Wi-Fi data to MySQL and generated the radio map. Because the modified GAN was required for input of the 2-D maps and the coordinates of APs, their information had to be secured. The 2-D map, essential for applying the modified GAN, was a 23x29-pixel image based on the reference points.

It was directly manufactured using CAD, as shown in Fig. 4.1 and Fig. 4.2. If a design drawing of the building can be secured as an image file, a separate indoor map-drawing process is unnecessary, and the size of the

image can be easily changed without any initial cost through the settings during pre-processing. In a corridor of the reference floor, the measured public APs from the walking survey were 8 APs out of 139. Their coordinates, the 2-D map image, and the Gaussian noise were input as initial learning data for the modified GAN. A setting of the 2-D map for learning assumed a line on the image to be a structure that completely blocked Wi-Fi signals. In contrast, the measured RSSIs of APs in the corridor spaces outside the boundaries were designed to estimate the Wi-Fi signal in a multi-path environment, reflected by its unique characteristics.

Generating a radio map used in the conventional fingerprint system required a simple arrangement of the measured RSSIs according to the reference points. This was unsuitable for the proposed UDRM, considering the spatial structure. Therefore, the structure of the radio map was reconfigured to fit the proposed UDRM, designed with the modified autoencoder and GAN.

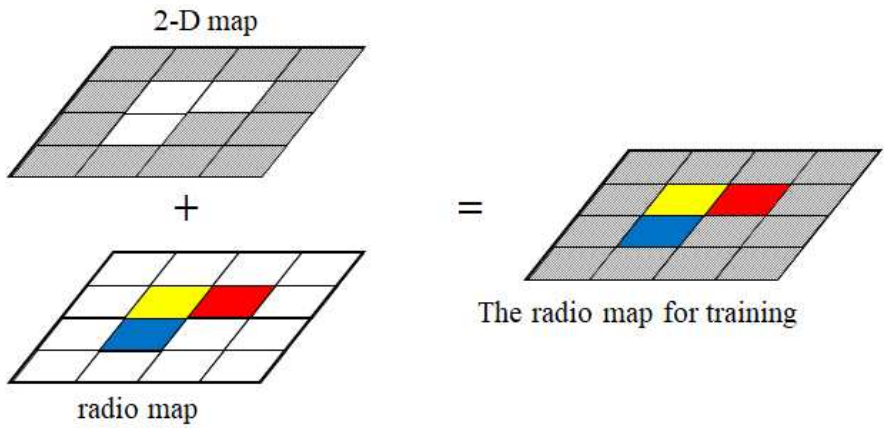

Fig. 4.4 The combined radio map for learning

Fig. 4.4 shows combined indoor structure and Wi-Fi radio maps. In the 2-D map on the upper left of the Fig. 4.4, the area represented by the hatching is a wall surface, and the remaining space for RSSIs is represented by the empty space. The radio map stores RSSIs up to the area where weak signals reach each reference point, and normalizes it to fit the neural network.

Unlike the conventional radio map, which is applied for fingerprint, the radio map applied to the proposed system is learned not only propagation characteristics but also indoor structures of the building. The real radio map of the reference floor as the input data used in the learning of the autoencoder, which were applied in similar areas and floors, remained the same. However, the outputs derived from the prediction of the autoencoder were interpolated, generating RSSIs that were not 100 % identical. Therefore,

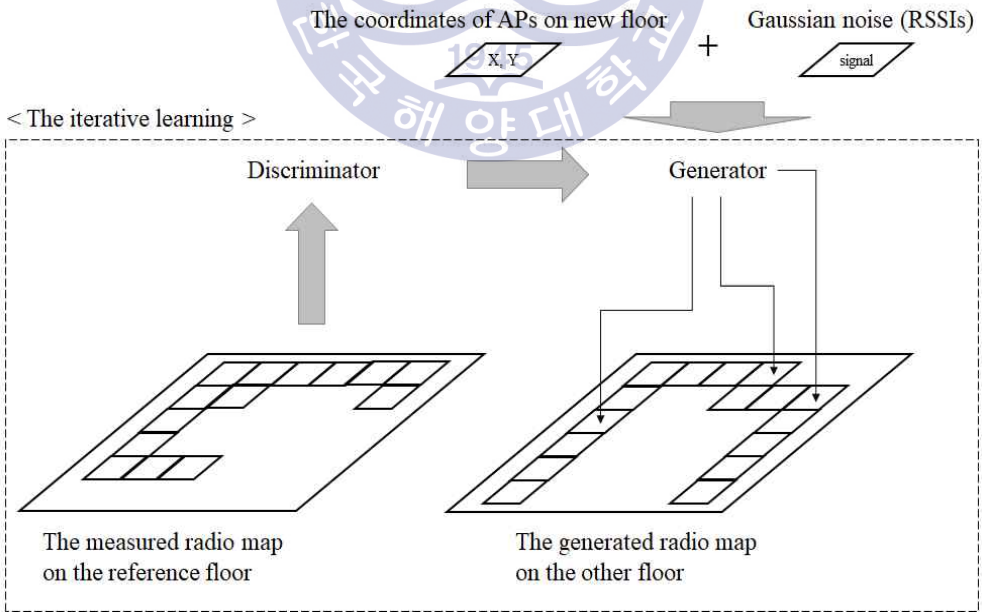

Fig. 4.5 The iterative learning of GAN

the radio map was preferentially generated using fake RSSIs, which linearly approximated the attenuation of the RSSI. Then, the generated RSSIs were inputted at the coordinates of the APs and a modified autoencoder-based radio map was finally completed.

Unlike the autoencoder method, the real measured radio map was not used as input data in the generator of modified GAN. The modified GAN applied areas where AP coordinates and indoor structures were difficult to estimate from the 2-D map, coordinates of APs, and Gaussian noise.

Fig. 4.5 shows the input and output data structure of the modified GAN. The coordinates on the left side are the location coordinates obtained by converting those of the real APs to the reference points. The spaces other than the indoor structures were subject to the estimated RSSIs through the GAN by inputting Gaussian noise.

4.2 Results of Unsupervised Dual Radio Mapping Algorithm

To verify the performance of the proposed UDRM, comprised of the modified autoencoder and GAN, the generated radio map was compared and analyzed with the real radio map measured from the walking survey.

Fig. 4.6 shows the result of the real RSSIs of measured APs on the reference floor and the result of the predicted RSSIs using the modified autoencoder in the corresponding of coordinate the AP. One pixel on the x and y-axes is an interval of 3 m on the 2-D map plane. (a) shows the real measured radio map by the walking survey. (b) shows the generated radio map predicted by the modified autoencoder on the 2nd floor. The RSSIs of the propagated Wi-Fi signal from the AP in the corridor is expressed in color

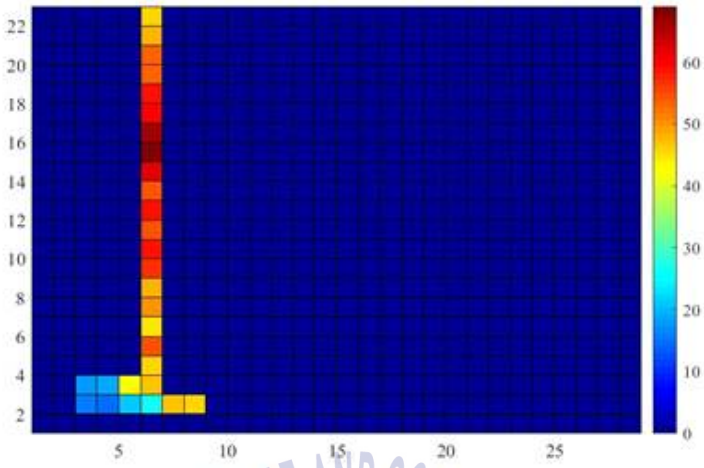

(a) The measured radio map

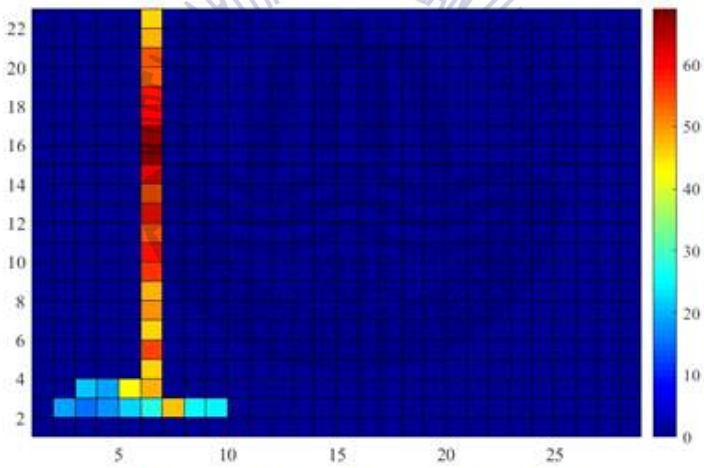

(b) The generated radio map (Autoencoder)

Fig. 4.6 The result of radio map by modified autoencoder (2nd floor)

intervals of 3 m to the reference points. Those expressed in red color are stronger. Blue color indicates a weaker signal. Based on the AP coordinates, the real RSSIs and the modified autoencoder-based radio map are replicated almost identically. However, differences between the predicted and measured

RSSIs occurred when the relative distance from the AP coordinate was more than 30 m. Because the AP signal is measured weaker when the distance is longer, the indoor interval where the RSSI of the Wi-Fi was measured from -90 to –100 dBm was reduced by the number of measurements, compared to the RSSI of the other strong Wi-Fi. That is, whereas the same number of times was measured, APs with strong signal strength measured closer to 100 %. APs with weak signal intensity had relatively low collection rates, compared to the number of measurements. Therefore, because it was difficult to acquire a sufficient measurement signals in the area where the RSSI was weak, per the increasing relative distance between the AP and the reference point, a difference occurred in the amount of learning, causing an error between the real measured radio map and the generated radio map by learning.

Fig. 4.7 shows the generated radio map of the 3rd floor by the measured RSSIs of the 2nd floor. One pixel on the x and y-axis is an interval of 3 m on the 2-D map plane. (a) shows the real measured radio map by the walking survey. (b) shows the generated radio map by the modified autoencoder on the 3rd floor. The 2nd and 3rd floors acquired nearly the same radio map, because the indoor structures and the coordinates of AP were the same. Analyzing this result in detail, unlike Fig. 4.6, the AP shows a unique signal result: an RSSI measured at an unexpected location, P. This is the result a unique indoor structure where RSSIs by a window cannot be measured sequential distance. Since P is a relatively large distance from the AP, the error occurs.

However, it can be confirmed that the signal measured in the unexpected area by the indoor structure predicted almost similarly to P'. K represents a

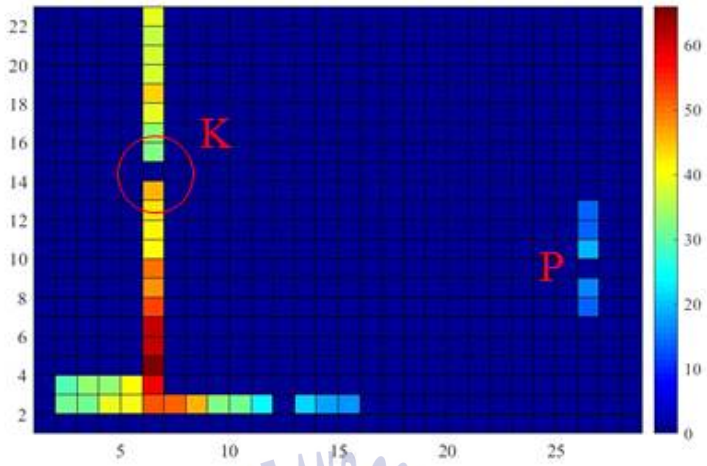

(a) The measured radio map

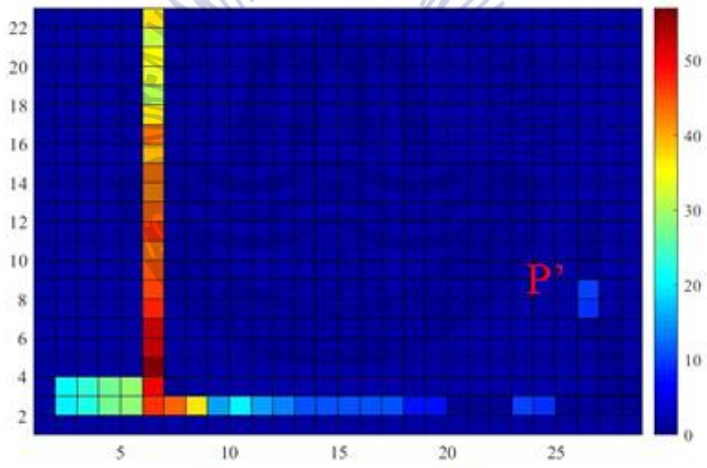

(b) The generated radio map (Autoencoder)

Fig. 4.7 The result of radio map by modified autoencoder (3rd floor)

missing data space caused by non-receipt of the signal. This is often caused by the walking survey. Despite the existence of this space, the replicated Wi-Fi distribution generates an RSSI via prediction, indicating that the resilience against the missing signal is excellent.

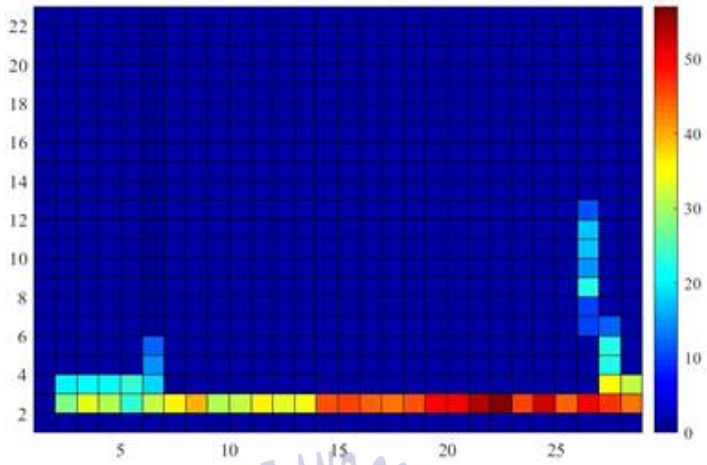

(a) The measured radio map

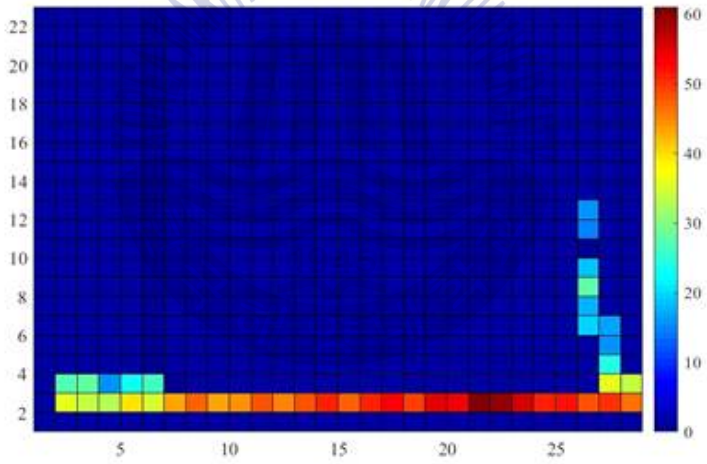

(b) The generated radio map (Autoencoder)

Fig. 4.8 The result of radio map by modified autoencoder (4th floor)

Fig. 4.8 (a) and (b) show the results of the measured radio map and the predicted radio map, based on the modified autoencoder on the 4th floor. The predicted radio map, (b), is similar to the previous Fig. 4.6 and Fig. 4.7, indicating that the prediction accuracy is slightly reduced in spaces where

RSSI is very weak.

Thus, the modified autoencoder can accurately predict the signals of AP in the area where the measured RSSIs are strong, and the predicted RSSI accuracy is lower in the area where the measured RSSIs are weak.

Because the relatively weak RSSI reduced the number of measurement, the same RSSI measurement time was used for the reference points for designing a radio map. There is a limit to increasing the measurement time at each reference point. However, if the RSSIs per reference points of all the APs were designed as a radio map, there would be many measured APs with strong signals, and the influences on the positioning would be relatively reduced.

Fig. 4.9 (a) and (b) show the measured radio map and the predicted radio map based on the modified GAN on the 5th floor. One pixel on the x and y-axes indicates an interval of 3 m on the 2-D map plane. The 5th floor has fewer public APs and a different floor plan, and the indoor area is smaller. Compared to Fig. 4.8, the coordinate of the AP is slightly different. Because the right area is outdoors, the AP is arranged to cover the indoor area. Thus, the RSSIs that learned from the reference floor only containing the indoor space became an area excluded from prediction, because it cannot learn about RSSI characteristics in the outdoor environment. The unlearned area is interpolated through the proposed MDLP-based RMF algorithm in the positioning phase. The 5th floor is different from the other floors, based on indoor structures. However, because learning is done using various kernels,

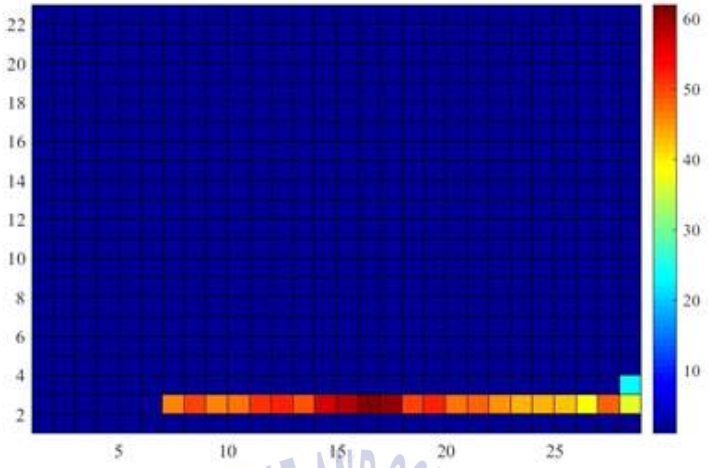

(a) The measured radio map

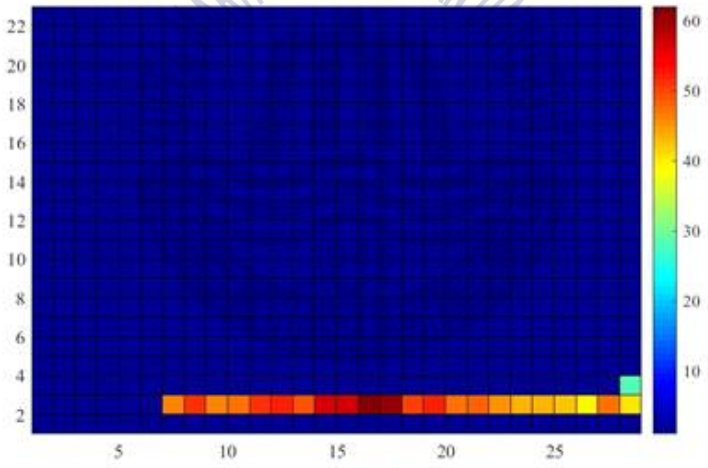

(b) The generated radio map (GAN)

Fig. 4.9 The result of radio map by modified GAN (5th floor)

as shown in Fig. 3.7, all those other than 1x1 are applied to combine the RSSI and the indoor structures. Therefore, the modified GAN also shows that the predicted radio map is similar to the real radio map only when the coordinates of APs are input exactly like the autoencoder.

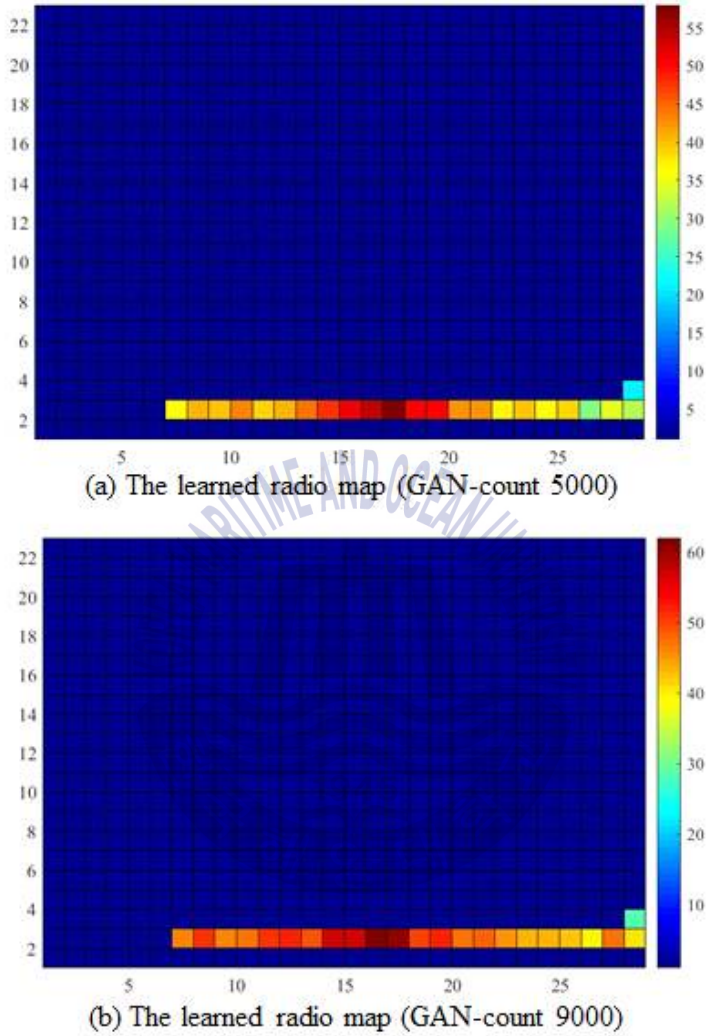

Fig. 4.10 The comparison of the radio map according to iterative learning count of the modified GAN

Fig. 4.10 shows the accuracy of the predicted radio map based on the modified GAN, according to the amount of learning. (a) shows the result of predicting the radio map using the generator through 5,000 learning iterations,

and (b) shows the result of predicting the radio map using the generator through 9,000 learning iterations. This result shows that not only the obtained RSSIs from the reference floor, but also the amount of learning, are important factors for prediction, because the measured RSSI does not have a constant value at one reference point. The difference in learning makes predicting the radio map slower, but the time can be drastically reduced, compared to the generation process of the radio map from the walking survey. The RSSIs of each AP were digitized and created as the radio map and stored in MySQL to complete preparation for interworking with a smartphone. The size of the predicted radio map through the proposed UDRM was 42x54. The x-axis is the relative RSSI, according to the distance between the AP and reference points. The y-axis represents the SSID of AP.

The predicted radio map of the UDRM was compared to the real measured radio map as follows.

Fig. 4.11 shows the errors between the results of the predicted radio map and the measured radio map, on the 2nd and 3rd floors. The x-axis represents the reference points, and the y-axis represents the error rate of the RSSIs. Because the distance at which the signal is measured varies according to the indoor structures and the installation coordinate of the corresponding AP, the size of the x-axis differs. In (a), the error occurs nearly 30 % at the three reference points. However, because the average error for all reference points is as low as 10 %, a positioning error may occur at a specific location. Because the measured RSSIs in various APs are used for positioning at one reference point, this error rate does not indicate a positioning error.

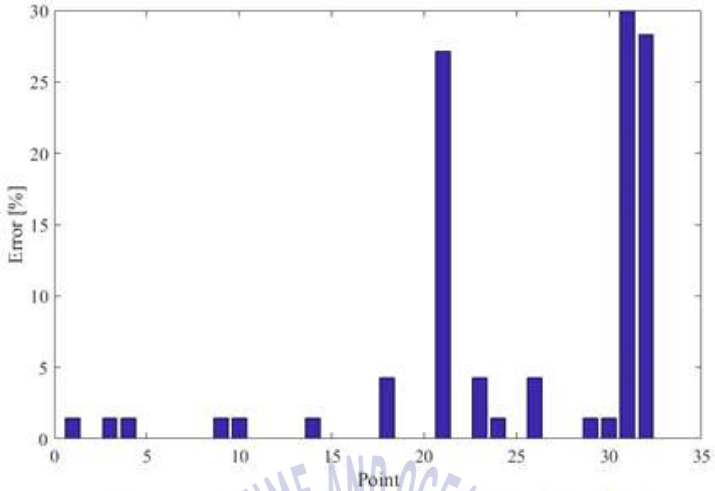

(a) The error rate of radio map by the 4th AP(2nd floor)

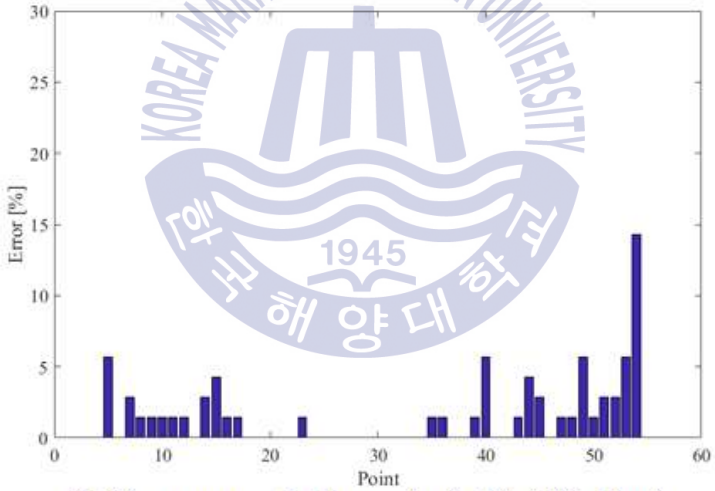

(b) The error rate of radio map by the 2th AP(3rd floor)

Fig. 4.11 The accuracy of generated RSSI on the 2nd and 3rd floors

Fig. 4.12 shows the accuracy of the predicted radio map on the 4th and 5th floors. (a) shows the error rate of the predicted radio map on the 4th floor by the modified autoencoder, and (b) shows the error rate on the 5th

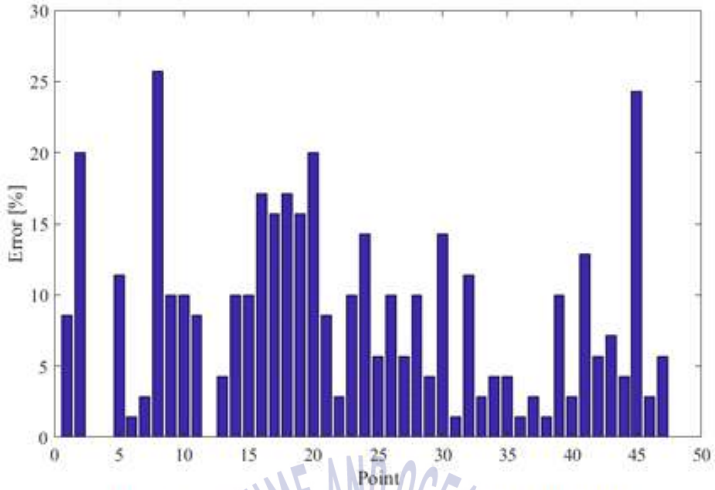

(a) The error rate of radio map by the 4th AP(4th floor)

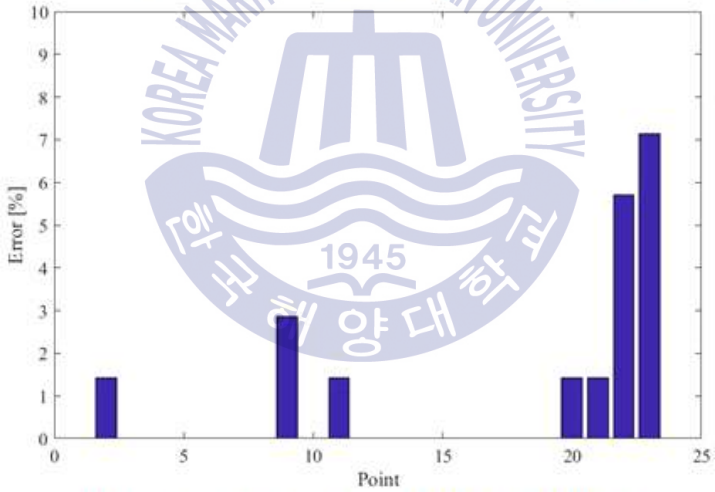

(b) The error rate of radio map by the 2th AP(5th floor)

Fig. 4.12 The accuracy of generated RSSI on the 4th and 5th floors

floor by the modified GAN. (a) shows the lowest performance of the predicted radio map among the AP signals on the fourth floor, and the average error rate is 9.67 % (less than 10 %). (b) shows that the performance

of the modified GAN is excellent, even if the position and the indoor space of the AP are changed by predicting the RSSIs nearly perfectly.

Table 4.1 shows the error rate of the predicted radio map for each floor. The total error rate of the generated radio map for each floor by the modified autoencoder is within 10 %, and the modified GAN on the 5thfloor is almost the same that the measured radio map: about 1 %.

Because these results fall within ranges less than 10 %, we have a stable error rate to prevent over-fitting. Despite these errors, there is an effect of Table 4.2 shows the accuracy of the two type radio maps generated by the UDRM. As a result of applying the algorithm to generate the radio map for all floors, when the directly measured radio map based on the walking

Table 4.1 The generation error rate of radio map on each floor

Floors	**2nd**	**3rd**	**4th**	**5th**
The prediction error rate of RSSIs	6.74 %	4.42 %	9.67 %	0.97 %

Table 4.2 The accuracy of radio map according to the UDRM

Algorithms	**The modified autoencoder**	**The modified GAN**
The radio map accuracy	90.40 %	92.70 %

Table 4.3 The algorithm processing speed according to the iterations

Algorithms	1 batch	20 batch	20 batch / 5000 times
Autoencoder	334 μsec/$step$	2 $msec/step$	18.12 min
GAN	1 $msec/step$	8 $msec/step$	65.40 min

survey is set the reference to 100 %, the modified autoencoder and the modified GAN are 90.40 % and 92.70 %, respectively. Whereas there is a limitation in generating an exact 100 % radio map, the error rates of the two algorithms were 9.6 % and 7.3 %, respectively, and were within the range of 5 to 10 %, which is a stable error rate for a general learning network. In conclusion, the UDRM results confirm that a stable system is an aspect of neural networks.

Table 4.3 shows the computation time of the proposed algorithms according to the size of the dataset using the proposed algorithm. A batch represents part of the total data, and an epoch represents the number of iterations of data. In the proposed algorithm, 120 epochs (the size of all RSSIs) were divided into 20 epochs each to prevent over-fitting instead of slowing down the operation, even if it were to increase the number of RSSI data for learning. However, decreasing the epoch increases the computation speed, but it causes over-fitting owing to the stronger data characteristic of each epoch.

Therefore, the 20 epochs were repeated 5,000 times in the proposed

UDRM, and total learning time was 18.12 *min* for the modified autoencoder and 65.40 *min* for the modified GAN. Thus, the autoencoder showed a relatively fast processing speed. In a 1 time operation, the processing speed of the two algorithms was 3 times the difference. However, in the case of 20 time operations, the difference was 4 fold. Thus, the difference of processing speed also increased with the number of operations. Owing to the structural characteristics of the GAN, the processing speed increased sharply with the number of operations. The modified autoencoder had a nearly constant learning time when the iteration count was 5,000. However, the modified GAN took 65.40 *min* less than the expected time, because the generator had learned, and the operation speed was faster.

Therefore, the time–cost required to create the radio map based on proposed UDRM in a building, except the first floor, was less than 2 *hrs*.

4.3 Result of MDLP-based Radio Map Feedback Algorithm

To update the Wi-Fi data measured simultaneously during positioning, measurement, and analysis phases, experiments were conducted to verify the proposed MDLP-based RMF algorithm.

Fig. 4.13 shows the result of outputting an IG for each AP using the radio map based on the modified autoencoder. The x-axis represents the number of personal APs measured on the 2nd floor and the y-axis represents the IG values of the corresponding APs. IG is a measure of independence within a group of APs or RSSIs. The measurement results not adapting the MDLP appear only as IG values on the 2nd floor. Therefore, all 170 APs

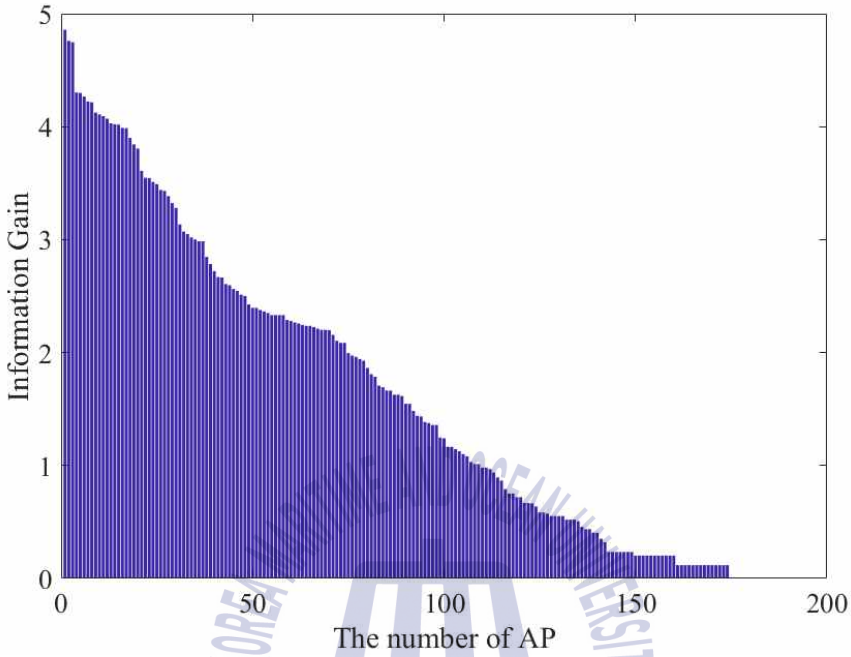

Fig. 4.13 The IG results of measured APs on the 2nd floor

measured on the 2nd floor were expressed as IG values without being removed.

Fig. 4.14 shows the result of AP removal by MDLP. the x-axis represents the number of personal APs measured on the 2nd floor, and the y-axis represents the IG values of the corresponding APs. Compared to the results shown in Fig. 4.13, the proposed MDLP removes 90 of the 170 APs. During this process, the measured radio map is input as-is, in real-time. The side-effect of the radio map taking an indiscriminate update is prevented in advance. Thus, only the necessary APs were added to the radio map. Through the gradual slope of the IG values of Fig. 4.13, it can be deduced that the distributions of RSSIs and the indoor structures of the 2nd floor were

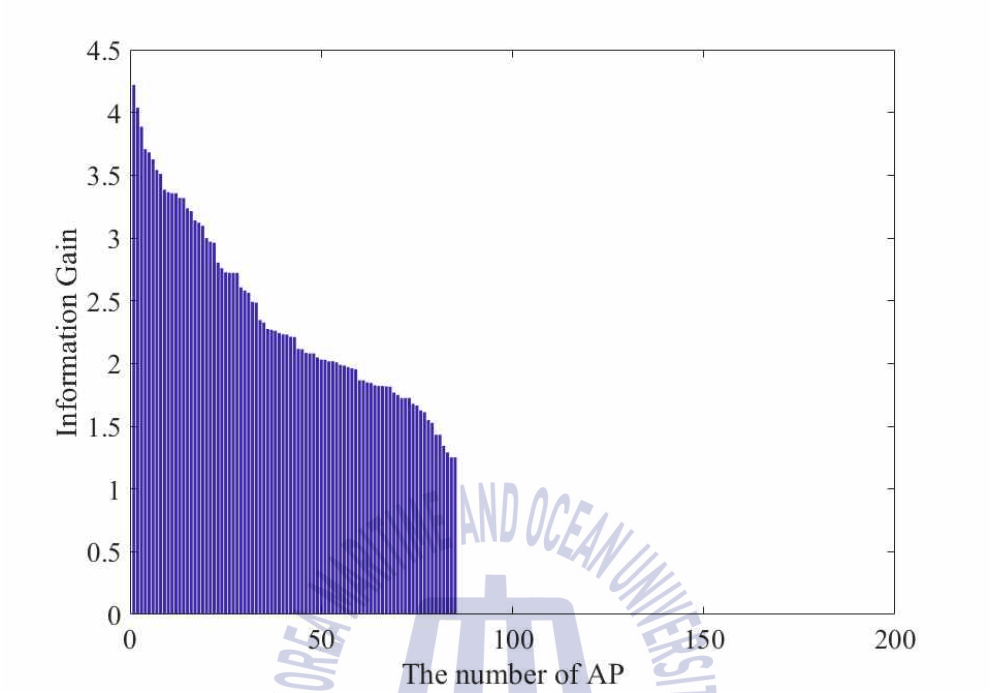

Fig. 4.14 The MDLP results of measured APs on the 2nd floor

not very complicated.

APs having very low IG values were removed by the proposed MDLP, because the change in RSSIs was small overall and was difficult to distinguish from reference points. Additionally, the APs were well-separated, but the RSSIs lacked continuity. Thus, the APs having large IG values were clustered with APs having similar RSSI distributions. Otherwise, the APs having the same RSSI randomly appeared at other reference points. Therefore, the IG value was not a criterion for the removal of the APs, but was a technique for visually confirming the RSSIs of an AP. Their removal was determined by the MDLP, according to the continuity of RSSIs and the distribution of APs.

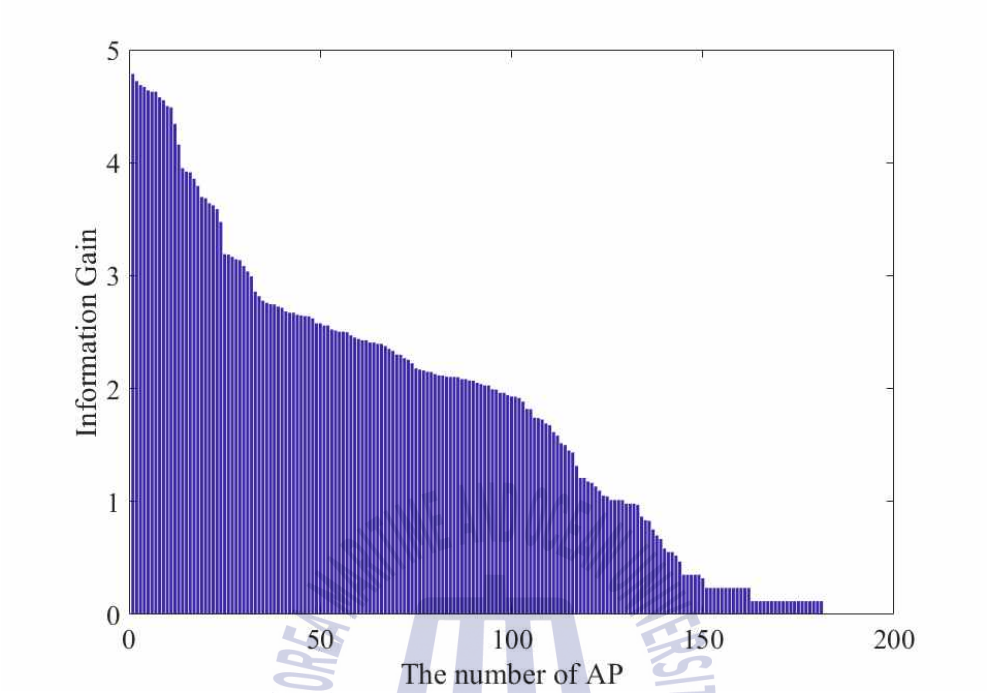

Fig. 4.15 The IG results of measured APs on the 3rd floor

Fig. 4.15 shows the result of IG analysis for each AP using the radio map based on the modified autoencoder on the 3rd floor. The x-axis represents the number of measured APs on the 3rd floor and the y-axis represents the IG of the corresponding APs. The APs not using the MDLP on the 3rd floor were not removed, resulting is almost the same configuration as the 2nd floor. From the slope of the IG values, it is possible to confirm that the AP distribution is partially deflected, unlike the 2nd floor. Fig. 4.16 shows the result of APs removal by MDLP and IG on the 3rd floor.

Compared to the results in Fig. 4.14, the proposed MDLP removed 77 of 181 APs. Thus, the discretization of APs was high. These APs can update the positioning accuracy and cover the shadow area. Additionally, when compared

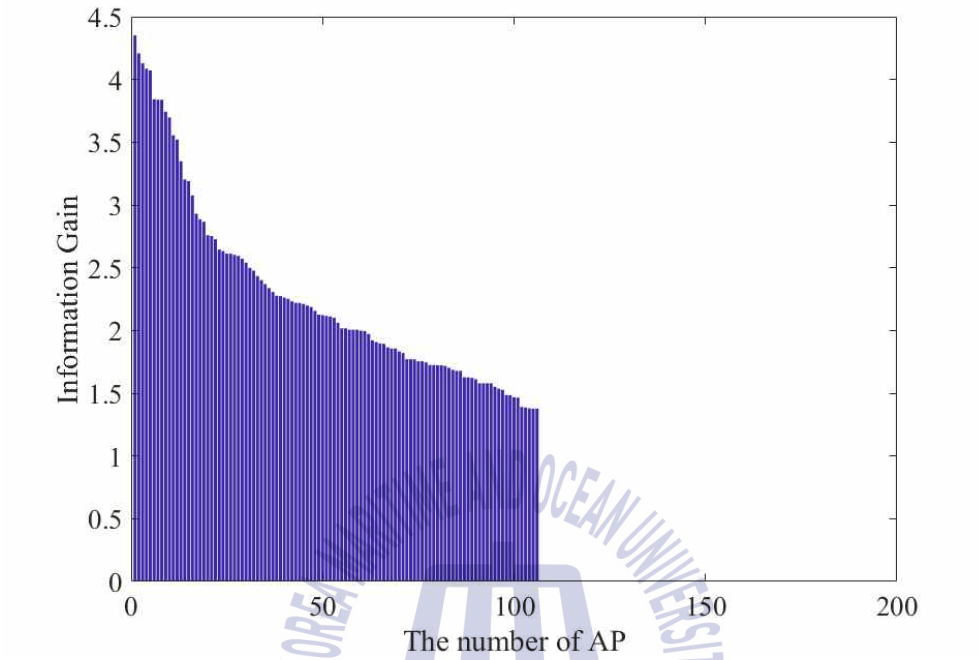

Fig. 4.16 The MDLP results of measured APs on the 3rd floor

with Fig. 4.14 and Fig. 4.15, the radio map to be updated is reduced by automatically deleting biased APs.

Fig. 4.16 shows the result of IG analysis for each AP using the radio map based on the modified GAN on the 5th floor. The x-axis represents the number of measured APs. The y-axis represents the IG of the corresponding APs. Only 75 signals were detected, unlike the number of measured APs on the other floors. Additionally, the measured APs on the 5th floor were updated via the same method as the other floors. In Fig. 4.16, the IG values were spread out evenly, and the number of measured APs on the 5th floor was much smaller than that of the 2nd, 3rd, and 4th floors. The distribution was very stable.

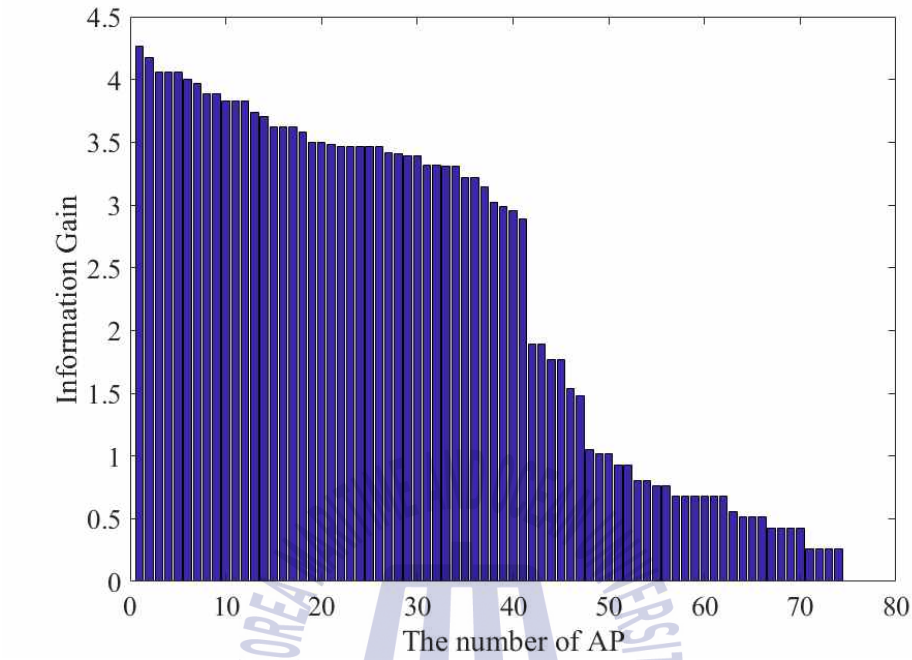

Fig. 4.17 The IG results of measured APs on the 5th floor

Fig. 4.17 shows the result of IG analysis for each APs using the radio map based on the modified GAN on the 5th floor. The x-axis represents the number of measured APs and the y-axis represents the IG of the corresponding APs. It can be seen that only 75 signals are detected, unlike the number of measured APs on other floors. In addition, the measured APs on the 5th floor are updated in the same method as the other floors. In Fig. 4.16, the IG values are spread out evenly, and the number of measured APs on the 5th floor is much smaller than that on the 2nd, 3rd, and 4th floors, and the distribution is very stable.

Fig. 4.18 shows the result of APs removal by MDLP and IG using the

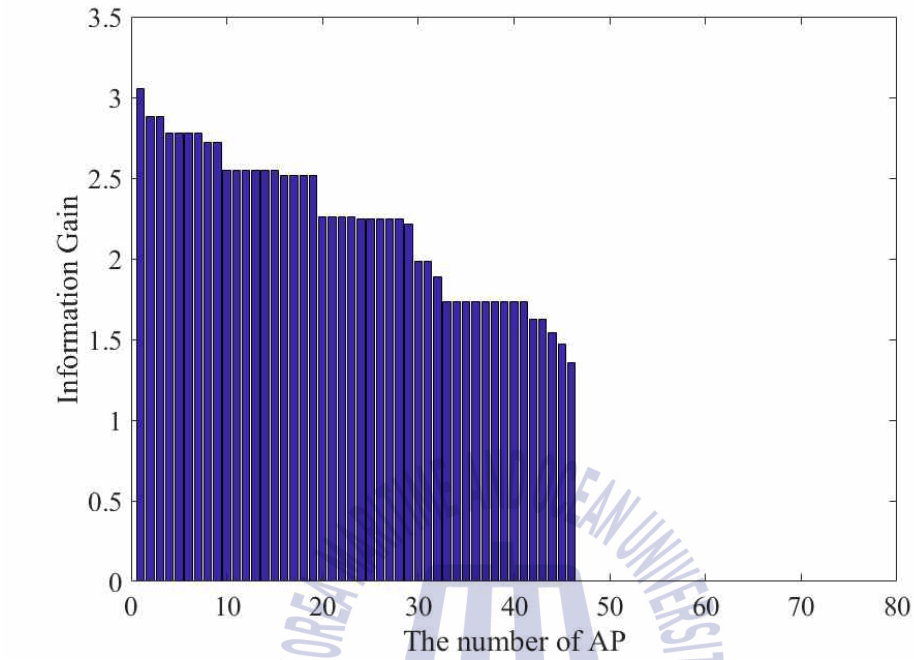

Fig. 4.18 The MDLP results of measured APs on the 5rd floor

radio map based on the GAN. It can be seen that the signal measured in Fig. 4.17 is finally reduced to 46 signals through the MDLP and IG.

Through these experimental results, the proposed MDLP-based RMF algorithm is confirmed and can be applied to APs on all floors, reducing their number by more than 50 % in the experimental building. The proposed algorithm can be applied in the training phase and shows excellent performance for data discretization via the continuity of RSSIs. In particular, the effect of discretization using MDLP is maximized in a space where AP distribution is spread evenly. Therefore, the proposed MDLP-based RMF algorithm is an optimization algorithm that prevents the rapid increase

Table 4.4 The euclidean distance based positioning accuracy to the walking survey based radio map and the proposed UDRM

Floor	The walking suervey based radio map	The proposed UDRM based radio map
2nd	86.07 %	80.25 %
3rd	88.36 %	85.19 %
4th	92.56 %	85.81 %
5th	89.73 %	85.61 %

of the radio map as the indoor AP increases, and it minimizes the degradation of the processing speed of positioning.

UDRM-based radio map and the walking survey-based radio map. It is confirmed that the positioning errors on the 2nd, 3rd, and 4th floors applied by the autoencoder were about 6 %, 3.2 %, and 6.8 %, respectively, which is still less than about 10 % of the map errors in the predicted radio map, based on UDRM. Because positioning was computed as the priority of the lower error rate of all APs rather than the error for each, the positioning accuracy was less affected than the RSSI error of the predicted AP. The acquired positioning result on the 5th floor had a low computation speed, but the positioning error rate was less than the other floors. Because the positioning result was applied to a different indoor structure, it was necessary to select the autoencoder and the GAN selectively, according to the indoor environment.

Table 4.5 The positioning results of MDLP applied radio maps

Floor	The measured radio map based positioning (The number of APs)	The measured radio map and MDLP based positioning (The number of APs)
2nd	90.00 % (248)	89.40 % (20)
3rd	89.12 % (248)	89.10 % (16)
4th	89.75 % (248)	89.74 % (20)
5th	89.77 % (248)	89.77 % (9)

Table 4.5 shows the positioning accuracy of MDLP applying the walking survey-based radio map and the UDRM-based radio map. When MDLP was applied based on 248 APs, which is the number of all APs measured between 2nd and 5th floors, the MDLP and IG were applied. The remaining APs were 20, 16, 20, and 9, respectively. When positioning was performed based on the euclidean distance algorithm, different sizes of APs were used, but the same positioning performance was obtained.

Table 4.6 shows the positioning result of the automatic Wi-Fi fingerprint system, based on unsupervised learning, combining UDRM and MDLP-based RMF algorithms. The positioning performance of the proposed system and the conventional fingerprint algorithm were, on average, 88.59 % and 89.66 %, respectively. The difference of positioning performance between the two systems was not nearly the same. This result is similar to the proposed algorithm, because the real radio map could not be 100 % correct,

Table 4.6 The positioning accuracy of the proposed fingerprint algorithm and the measured based fingerprint

Floor	The measured based fingerprint	The proposed fingerprint
2nd	90.00 %	90.00 %
3rd	89.12 %	88.77 %
4th	89.75 %	89.41 %
5th	89.77 %	86.17 %

owing to the inherent variation of RSSI. As this result shows, the conventional fingerprint produced a radio map of all the APs, and the proposed algorithm assumes that enough AP RSSIs were collected during the moving processes. If a user does not have sufficient updates, owing to insufficient movement, the positioning performance will be degraded. However, the same performance can be obtained when the data is sufficiently acquired by user movement, making it a very effective system for generating a radio map.

Chapter 5 Conclusion

To minimize the time taken to acquire Wi-Fi signals in automatic fingerprint systems when the indoor area becomes complicated and the size increases, we studied the radio characteristics of indoor environments based on unsupervised learning and proposed the combined UDRM and MDLP-based RMF algorithm. UDRM selects either the modified autoencoder or the modified GAN according to the indoor structure of each floor to improve the processing speed and to better predict the radio map. Because these algorithms use unsupervised learning, it is not necessary to create additional labeled data, making application easy, using the SSIDs and RSSIs of APs in the building. The concordance rates of the radio map generated by the proposed UDRM and the walking survey are relatively accurate, within 10 %. These errors of the radio map based on UDRM are within a very stable range from the viewpoint of a neural network-based learning algorithm, and the stability of the proposed UDRM is ensured by the concordance rates.

The MDLP-based RMF algorithm copes with changes (e.g., positioning, installation, and AP removal), reducing the time taken to acquire RSSIs by subordinating the generation process of the radio map in the training phase to the positioning phase. The experimental results of the proposed automatic Wi-Fi fingerprint system, based on unsupervised learning, are as follows.

In the proposed UDRM algorithm, the learning times of the 20 batches used for learning and prediction of the modified autoencoder and GAN-based

radio map were 2 *ms/step* and 8 *ms/step*, respectively. Thus, the modified GAN, which is more complex than the modified autoencoder, reduced the learning time by 4. Then, when the measured radio map based on the walking survey was 100 %, the concordance rates of the generated radio map obtained by the modified autoencoder and GAN were 90.4 % and 92.7 %, showing 9.6 % and 7.3 % prediction errors, respectively. These errors were at an ideal rate to prevent over-fitting caused by a high prediction accuracy of more than 95 % while training the neural network. Although the accuracy was lowered by about 10 %, compared to the measured radio map from the walking survey, the proposed system showed good performance, and the designed network is very stable as a neural network.

In the positioning phase, when the MDLP-based RMF algorithm was applied to the radio map of the modified autoencoder and GAN, the update rate of the radio map was 52.9 % and 60.5 %, respectively. Additionally, the positioning accuracy of the proposed fingerprint system was 88.59 %, compared to the 89.66 % accuracy obtained with the measured radio map based on the walking survey, showing that there was almost no error. In other words, the automatic Wi-Fi fingerprint system, based on unsupervised learning, reduced the radio map by 43.3 % on average, even when the positioning accuracy was almost the same. The time taken to acquire RSSIs and the workload are the biggest problems in fingerprinting; however, these can be significantly shortened by automatically updating and creating the radio maps.

Reference

[1] Anagnostopoulos, V., Havlena, M., Kiefer, P., Giannopoulos, I., Schindler, K., & Raubal, M., "Gaze-Informed location-based services", *International Journal of Geographical Information Science*, vol. 31, no. 9, pp. 1770-1797, 2017.

[2] Ray, S., Blanco, R., & Goel, A. K., "High performance location-based services in a main-memory database", *GeoInformatica*, vol. 21 no. 2, pp. 293-322, 2017.

[3] Nagarajan, S. G., Zhang, P., & Nevat, I., "Geo-spatial location estimation for Internet of Things (IoT) networks with one-way time-of-arrival via stochastic censoring", *IEEE Internet of Things Journal*, vol. 4, no. 1, pp. 205-214. 2017.

[4] Shalaby, M., Shokair, M., & Messiha, N. W., "Performance Enhancement of TOA Localized Wireless Sensor Networks", *Wireless Personal Communications*, vol. 95, no. 4, pp. 4667-4679, 2017.

[5] Daniel, O., Wymeersch, H., & Nurmi, J., "Delay‐Accuracy Tradeoff in Opportunistic Time-of-Arrival Localization", *IEEE Signal Processing Letters*, vol. 25, no. 6, pp. 763-767, 2018.

[6] Wu, C., Yang, Z., & Xiao, C., "Automatic radio map adaptation for indoor localization using smartphones", *IEEE Transactions on Mobile Computing*, vol. 17, no. 3, pp. 517-528, 2018.

[7] Luo, C., Cheng, L., Chan, M. C., Gu, Y., Li, J., & Ming, Z., "Pallas: Self-bootstrapping fine-grained passive indoor localization using WiFi monitors", *IEEE Transactions on Mobile Computing*, vol. 16, no. 2, pp. 466-481, 2017.

[8] Zuo, J., Liu, S., Xia, H., & Qiao, Y., "Multi-Phase Fingerprint Map Based on Interpolation for Indoor Localization Using iBeacons", *IEEE Sensors Journal*, vol. 18, no. 8, pp. 3351-3359, 2018.

[9] Zhuang, Y., Li, Y., Qi, L., Lan, H., Yang, J., & El-Sheimy, N., "A two-filter integration of MEMS sensors and WiFi fingerprinting for indoor positioning", *IEEE Sensors Journal*, vol. 16, no. 13, pp. 5125-5126, 2016.

[10] Jung, H. H. and Lee, K. S., "Indoor Positioning Method of a Motorcar Based on Chirp Spread Spectrum", *International Journal of Applied Engineering Research*, vol. 11, no. 2, pp. 1408-1413, 2016.

[11] Seong, J. H., Choi, E. C., Lee, J. S., & Seo, D. H., "High-speed positioning and automatic updating technique using Wi-Fi and UWB in a ship", *Wireless Personal Communications*, vol. 94, no. 3, pp. 1105-1121, 2017.

[12] Ruiz, A. R. J. and Granja, F. S., "Comparing Ubisense, BeSpoon, and DecaWave UWB location systems: indoor performance analysis", *IEEE Transactions on instrumentation and Measurement*, vol. 66, no. 8, pp. 2106-2117, 2017.

[13] Chen, G., Meng, X., Wang, Y., Zhang, Y., Tian, P., & Yang, H., "Integrated WiFi/PDR/Smartphone using an unscented kalman filter algorithm for 3D indoor localization", *Sensors*, vol. 15, no. 9, pp. 24595-24614, 2015.

[14] Wu, C., Yang, Z., & Liu, Y., "Smartphones based crowdsourcing for indoor localization", *IEEE Transactions on Mobile Computing*, vol. 14, no. 2, pp. 444-457. 2017.

[15] Wang, E., Wang, M., Meng, Z., & Xu, X., "A Study of WiFi-Aided Magnetic Matching Indoor Positioning Algorithm", *Journal of Computer and Communications*, vol. 5, no. 3, pp. 91-101, 2017

[16] Filonenko, V., Cullen, C., & Carswell, J. D., "Indoor positioning for smartphones using asynchronous ultrasound trilateration", *ISPRS International Journal of Geo-Information*, vol. 2, no. 3, pp. 598-620, 2013.

[17] Chen, K., Wang, C., Yin, Z., Jiang, H., & Tan, G., "Slide: Towards Fast and Accurate Mobile Fingerprinting for Wi-Fi Indoor Positioning Systems", *IEEE Sensors Journal*, vol. 18, no. 3, pp. 1213-1223, 2018.

[18] Chen, Q., Ding, D., & Zheng, Y., “Indoor pedestrian tracking with sparse RSS fingerprints”, *Tsinghua Science and Technology*, vol. 23, no. 1, pp. 95-103, 2018.

[19] Ren, Y., Salim, F. D., Tomko, M., Bai, Y. B., Chan, J., Qin, K. K., & Sanderson, M., “D-Log: A WiFi Log-based differential scheme for enhanced indoor localization with single RSSI source and infrequent sampling rate”, *Pervasive and Mobile Computing*, vol. 37, pp. 94-114, 2017.

[20] Park, T. R., Kim, T. H., Choi, J. Y., Choi, S., & Kwon, W. H., “ Throughput and energy consumption analysis of IEEE 802.15. 4 slotted CSMA/CA”, *Electronics Letters*, vol. 41, no. 18, pp. 1017-1019. 2005.

[21] Dinh, N. Q., & Kim, D. S. “Performance evaluation of priority CSMA-CA mechanism on ISA100. 11a wireless network”, *Computer Standards & Interfaces*, vol. 34, no. 1, pp. 117-123. 2012.

[22] Park, T. R., Kim, T. H., Choi, J. Y., Choi, S., & Kwon, W. H., “ Throughput and energy consumption analysis of IEEE 802.15. 4 slotted CSMA/CA”, *Electronics Letters*, vol. 41, no. 18, pp. 1017-1019. 2005.

[23] Mazlan, M. A. A. A., Khir, M. M., Saad, N. M., & Dass, S. C., “WiFi Fingerprinting Indoor Positioning with Multiple Access Points in a Single Base Station using Probabilistic Method”, *International Journal of Applied Engineering Research*, vol. 12, no. 6, pp. 1102-1113, 2017.

[24] Seong, J. H. and Seo, D. H., “Wi-Fi fingerprint using radio map model based on MDLP and euclidean distance based on the Chi squared test”, *Wireless Networks*, pp. 1-9, 2018.

[25] Seong, J. H. and Seo, D. H., “Environment Adaptive Localization Method Using Wi-Fi and Bluetooth Low Energy”, *Wireless Personal Communications*, vol. 99, no. 2, pp. 1-14. 2018.

[26] Wu, C., Yang, Z., & Liu, Y., “Smartphones based crowdsourcing for indoor localization”, *IEEE Transactions on Mobile Computing*, vol. 14, no. 2, pp. 444-457, 2015.

[27] Zhang, X., Wong, A. K. S., Lea, C. T., & Cheng, R. S. K.,

"Unambiguous Association of Crowd-sourced Radio Maps to Floor Plans for Indoor Localization", *IEEE Transactions on Mobile Computing*, vol. 17, no. 2, pp. 488-502, 2018.

[28] Luo, C., Hong, H., Chan, M. C., Li, J., Zhang, X., & Ming, Z., " MPiLoc: Self-Calibrating Multi-Floor Indoor Localization Exploiting Participatory Sensing", *IEEE Transactions on Mobile Computing*, vol. 17, no. 1, pp. 141-154. 2018

[29] Jung, S. H., Moon, B. C., & Han, D., "Performance evaluation of radio map construction methods for wi-fi positioning systems", *IEEE Transactions on Intelligent Transportation Systems*, vol. 18, no. 4, pp. 880-889, 2017.

[30] Bisio, I., Cerruti, M., Lavagetto, F., Marchese, M., Pastorino, M., Randazzo, A., & Sciarrone, A., "A trainingless wifi fingerprint positioning approach over mobile devices", *IEEE Antennas and Wireless Propagation Letters*, vol. 13, pp. 832-835. 2014.

[31] Gu, Z., Chen, Z., Zhang, Y., Zhu, Y., Lu, M., & Chen, A., "Reducing fingerprint collection for indoor localization", *Computer Communications*, vol. 83, pp. 56-63, 2016.

[32] Liu, H. H., "The quick radio fingerprint collection method for a wifi-based indoor positioning system", *Mobile Networks and Applications*, vol. 12, no. 1, pp. 61-71. 2017.

[33] Jiang, Q., Ma, Y., Liu, K., & Dou, Z., "A probabilistic radio map construction scheme for crowdsourcing-based fingerprinting localization", *IEEE Sensors Journal*, vol. 16, no. 10, pp. 3764-3774, 2016.

[34] Chow, K. H., He, S., Tan, J., & Chan, S. H. G., "Efficient Locality Classification for Indoor Fingerprint-based Systems", *IEEE Transactions on Mobile Computing*, 2018.

[35] Zhou, M., Tang, Y., Tian, Z., & Geng, X., "Semi-supervised learning for indoor hybrid fingerprint database calibration with low effort", *IEEE Access*, vol. 5, pp. 4388-4400. 2017.

[36] Wu, K., Xiao, J., Yi, Y., Chen, D., Luo, X., & Ni, L. M., "CSI-based

indoor localization", *IEEE Transactions on Parallel and Distributed Systems*, vol. 24, no. 7, pp. 1300-1309. 2013.

[37] Lin, T. N., Fang, S. H., Tseng, W. H., Lee, C. W., & Hsieh, J. W., "A group-discrimination-based access point selection for WLAN fingerprinting localization", *IEEE Transactions on Vehicular Technology*, vol. 63, no. 8, pp. 3967-3976. 2014.

[38] Wu, Z., Fu, K., Jedari, E., Shuvra, S. R., Rashidzadeh, R., & Saif, M., " A fast and resource efficient method for indoor positioning using received signal strength", *IEEE Transactions on Vehicular Technology*, vol. 65, no. 12, pp. 9747-9758. 2016.

[39] Zhou, R., Lu, X., Zhao, P., & Chen, J., "Device-Free Presence Detection and Localization With SVM and CSI Fingerprinting", *IEEE Sensors Journal*, vol. 17, no. 23, pp. 7990-7999. 2017.

[40] Patel, H. J., Temple, M. A., & Baldwin, R. O., "Improving zigbee device network authentication using ensemble decision tree classifiers with radio frequency distinct native attribute fingerprinting", *IEEE Transactions on Reliability*, vol. 64, no. 1, pp. 221-233. 2015.

[41] Jia, B., Huang, B., Gao, H., & Li, W., "Dimension reduction in radio maps based on the supervised kernel principal component analysis", *Soft Computing*, pp. 1-7. 2018.

[42] Ropero, R. F., Renooij, S., & van der Gaag, L. C., "Discretizing environmental data for learning Bayesian-network classifiers", *Ecological Modelling*, vol. 368, pp. 391-403. 2018.

[43] Wen, L. Y., Min, F., & Wang, S. Y., "A two-stage discretization algorithm based on information entropy", *Applied Intelligence*, vol. 47, no. 4, pp. 1169-1185, 2017.

[44] Uğuz, H., "A two-stage feature selection method for text categorization by using information gain, principal component analysis and genetic algorithm", *Knowledge-Based Systems*, vol. 24, no. 7, pp. 1024-1032, 2011.

[45] Krizhevsky, A., Sutskever, I., & Hinton, G. E., "Imagenet classification

with deep convolutional neural networks", *In Advances in neural information processing systems*, pp. 1097-1105, 2012.

[46] Shin, H. C., Roth, H. R., Gao, M., Lu, L., Xu, Z., Nogues, I., ... & Summers, R. M., "Deep convolutional neural networks for computer-aided detection: CNN architectures, dataset characteristics and transfer learning", *IEEE transactions on medical imaging*, vol. 35, no. 5, pp. 1285-1298, 2016.

[47] Kim, K. S., Lee, S., & Huang, K., "A scalable deep neural network architecture for multi-building and multi-floor indoor localization based on Wi-Fi fingerprinting", *Big Data Analytics*, vol. 3, no. 1, 2018.

[48] Merchant, K., Revay, S., Stantchev, G., & Nousain, B., "Deep learning for RF device fingerprinting in cognitive communication networks", *IEEE Journal of Selected Topics in Signal Processing*, vol. 12, no. 1, pp. 160-167, 2018.

[49] Huang, F. J., Boureau, Y. L., & LeCun, Y., "Unsupervised learning of invariant feature hierarchies with applications to object recognition", *IEEE Conference on Computer Vision and Pattern Recognition 2007*, pp. 1-8, 2007.

[50] Erhan, D., Bengio, Y., Courville, A., Manzagol, P. A., Vincent, P., & Bengio, S., "Why does unsupervised pre-training help deep learning?", *Journal of Machine Learning Research*, pp. 625-660, 2010.

[51] Schmidhuber, J., "Deep learning in neural networks: An overview", *Neural networks*, vol. 61, pp. 85-117. 2015.

[52] Goodfellow, I., Pouget-Abadie, J., Mirza, M., Xu, B., Warde-Farley, D., Ozair, S., Courville A., & Bengio, Y., "Generative adversarial nets", *In Advances in neural information processing systems*, pp. 2672-2680, 2014.

[53] Chen, X., Duan, Y., Houthooft, R., Schulman, J., Sutskever, I., & Abbeel, P., "Infogan: Interpretable representation learning by information maximizing generative adversarial nets", *In Advances in Neural Information Processing Systems*, pp. 2172-2180. 2016.